

# Vulnerability in a Tropical Cyclone Risk Model: Philippines Case Study

Jane W. Baldwin<sup>1</sup>, Chia-Ying Lee<sup>2</sup>, Brian Walsh<sup>3</sup>, Suzana Camargo<sup>2</sup>, and Adam Sobel<sup>4</sup>

<sup>1</sup>Department of Earth System Science, University of California Irvine

<sup>2</sup>Lamont-Doherty Earth Observatory, Columbia University

<sup>3</sup>World Bank

<sup>4</sup>Columbia University

November 22, 2022

## Abstract

The authors describe a tropical cyclone risk model for the Philippines, using methods that are open-source and can be straightforwardly generalized to other countries. Wind fields derived from historical observations, as well as those from an environmentally forced tropical cyclone hazard model (using environmental forcing from the recent historical period) are combined with data representing exposed value and vulnerability to determine asset losses. Exposed value is represented by the LitPop dataset, which assumes total asset value is distributed across a country following population density and nightlights data. Vulnerability is assumed to follow a functional form previously proposed by Emanuel, with free parameters chosen by a sensitivity analysis in which simulated and historical reported damages are compared for different parameter values. Use of different vulnerability parameters for the region around Manila yields much better agreement between simulated and actually reported losses than does a single set of parameters for the entire country. Even then, however, the model predicts no losses for a substantial number of historical storms which did in fact produce them, a difference the authors hypothesize is at least in part due to the use of wind speed as the sole metric of TC hazard, omitting explicit representation of flooding due to storm surge and/or rainfall.

1 **Vulnerability in a Tropical Cyclone Risk Model: Philippines Case Study**

2 Jane W. Baldwin\*

3 *Department of Earth System Science, University of California Irvine, Irvine, California*

4 Chia-Ying Lee

5 *Lamont-Doherty Earth Observatory, Palisades, New York*

6 Brian J. Walsh

7 *World Bank, Washington, D.C.*

8 Suzana J. Camargo

9 *Lamont-Doherty Earth Observatory, Palisades, New York*

10 Adam H. Sobel

11 *Columbia University, New York, New York*

12 \*Corresponding author: Jane W. Baldwin, jane.baldwin@uci.edu

## ABSTRACT

13 The authors describe a tropical cyclone risk model for the Philippines, using methods that are  
14 open-source and can be straightforwardly generalized to other countries. Wind fields derived  
15 from historical observations, as well as those from an environmentally forced tropical cyclone  
16 hazard model (using environmental forcing from the recent historical period) are combined with  
17 data representing exposed value and vulnerability to determine asset losses. Exposed value is  
18 represented by the LitPop dataset, which assumes total asset value is distributed across a country  
19 following population density and nightlights data. Vulnerability is assumed to follow a functional  
20 form previously proposed by Emanuel, with free parameters chosen by a sensitivity analysis in  
21 which simulated and historical reported damages are compared for different parameter values. Use  
22 of different vulnerability parameters for the region around Manila yields much better agreement  
23 between simulated and actually reported losses than does a single set of parameters for the entire  
24 country. Even then, however, the model predicts no losses for a substantial number of historical  
25 storms which did in fact produce them, a difference the authors hypothesize is at least in part due to  
26 the use of wind speed as the sole metric of TC hazard, omitting explicit representation of flooding  
27 due to storm surge and/or rainfall.

28 *Significance statement.* Landfalling tropical cyclones are devastating disasters in terms of their  
29 loss of property and life. The Philippines is particularly at risk for these disasters. Here we develop  
30 a model for tropical cyclone risk, e.g. property losses, over the Philippines, and demonstrate its  
31 effectiveness by comparing to historical observations. We find that capturing the difference in  
32 vulnerability between the largest city in the Philippines (Manila) and more rural areas is important  
33 to accurately model tropical cyclone risks. Using this model, we can more accurately simulate the  
34 risk of very extreme tropical cyclone events in the Philippines. The model can also easily be applied  
35 to other countries and for climate change scenarios using information that is openly available. Our  
36 model does not accurately capture damages from storms dominated by flooding instead of wind,  
37 and future work should improve this aspect of the model. Nonetheless, the existing model is useful  
38 for emergency planning and adaptation, especially in lower income countries where data is limited.

## 39 **1. Introduction**

40 Accurate assessments of tropical cyclone (TC) risk are valuable for disaster risk reduction and  
41 climate adaptation. Such assessments can inform decisions about both where to build resilience  
42 and emergency preparedness prior to TC-induced disasters and where to allocate aid following such  
43 disasters, and can also inform the development of insurance and reinsurance products. Assessing  
44 risk requires consideration of three different factors (Field et al. 2012). The first factor is the  
45 hazard. The hazard characterizes the probabilities that given levels of geophysical variables —  
46 e.g., wind speed, rainfall, storm surge — will be exceeded. The second factor is the exposure,  
47 which characterizes the human, structural, or agricultural assets in a place which might be affected  
48 by the disaster. The third factor is vulnerability, which is the degree to which those assets will  
49 be lost if one or more of the geophysical variables exceeds a given value. TC risks are typically  
50 quantified in the form of asset losses, or the replacement cost of assets destroyed by a TC event.

51 Over the past decade or so, significant strides have been made in quantifying different aspects  
52 of TC risk. Given that TCs — particularly the few most intense ones that cause the largest share  
53 of damage — are rare events, the observed historical record is too limited for accurate TC risk  
54 assessment. Statistical-dynamical models have been developed that allow the simulation of many  
55 physically plausible TCs given background environmental conditions (Emanuel 2011; Lee et al.  
56 2018; Jing and Lin 2020; Bloemendaal et al. 2020b). Synthetic TCs generated by such models  
57 are used for assessment of extreme wind hazards (Sobel et al. 2019; Bloemendaal et al. 2020a),  
58 coupled with hydrodynamical models to estimate storm surge hazards (Lin et al. 2010; Lin and  
59 Chavas 2012), and coupled with physics-based models of precipitation to estimate extreme rainfall  
60 hazards (Xi et al. 2020; Gori et al. 2022).

61 Alongside these advances in modeling TC hazards, progress has been made in modeling TC  
62 vulnerability and exposure. This work can be broadly categorized into structural, economic, and  
63 social approaches (Wilson and Baldwin 2021). For the USA, FEMA’s Hazus model provides a  
64 relatively comprehensive framework for modeling wind and flood risks, including computation  
65 of exposure and vulnerability from building maps and structural engineering principles (Vickery  
66 et al. 2006b,a). Some information in Hazus, especially around vulnerability of building types,  
67 has been adapted for use in other countries by the UNISDR’s Global Assessment Reports (Yamin  
68 et al. 2014). However, the lack of detailed building maps and complexity of Hazus does limit its  
69 applicability to other countries. In contrast, recent studies using more top-down, economic-based  
70 approaches have created global exposure fields and country-scale impact functions for TC risk  
71 modeling (Eberenz et al. 2020b,a). While these methods are more simplified than Hazus, they have  
72 the advantage of being consistently applicable across the globe. Vulnerability can also be estimated  
73 based on population characteristics (what we term “social approaches”) (Cutter et al. 2003; Tellman  
74 et al. 2020; Dominguez et al. 2021). While these techniques are suitable for assessing relative

75 vulnerabilities of different regions (e.g. counties), existing social approaches are somewhat less  
76 straightforward to merge with TC hazard and exposure for quantitative risk assessment.

77 A key challenge for TC risk assessment is incorporating changing hazards following climate  
78 change. As carbon concentrations in the atmosphere increase and the global climate warms,  
79 TCs and their related hazards may be altered in a variety of ways. There is high confidence  
80 that rising sea levels will lead to greater storm surge, medium to high confidence that TC-related  
81 precipitation will increase, and medium to high confidence that TC intensity will increase (Knutson  
82 et al. 2020). Other aspects of TC change are more uncertain. For example, there is ongoing  
83 debate about how the overall frequency of TCs will change with global warming (Vecchi et al.  
84 2019), though somewhat more confidence that the frequency of the most intense (i.e. Category  
85 4 or 5 storms) will increase. Traditionally, hurricane risk assessment has been based primarily  
86 on historical tracks (Watson and Johnson 2004), but this approach is not appropriate in a non-  
87 stationary climate. In contrast, the previously discussed statistical-dynamical approaches can be  
88 applied with environmental conditions drawn from climate change scenarios to estimate changing  
89 hazards from TCs (Emanuel 2011; Lee et al. 2020); this method presents an important way forwards  
90 in estimating present and future TC risk. However, to fully capture TC risks in a changing climate  
91 also requires consideration of the compound hazards associated with these storms (Leonard et al.  
92 2014; Zscheischler et al. 2018). Wind, precipitation, surge, rising temperatures and sea levels all  
93 play roles in changing TC risks and studies are beginning to consider these changing hazards in  
94 concert (Lin et al. 2012; Matthews et al. 2019; Gori et al. 2022).

95 Another challenge for TC risk assessment, and disaster risk assessment in general, is quantita-  
96 tively capturing impacts on human welfare. Disasters have been shown to disproportionately effect  
97 poorer countries (Noy 2009). In the Philippines in particular, typhoons disproportionately effect  
98 poorer individuals and children, in terms of educational, economic, and health impacts (Deuchert

99 and Felfe 2015; Sakai et al. 2017; Yonson et al. 2018). Traditional quantification of asset losses  
100 cannot account for these differential impacts across the income distribution. Indeed, asset losses  
101 may more readily reflect the impact on wealthy individuals who own the most assets, as opposed to  
102 poorer individuals whose welfare can be more gravely affected by a given disaster (Hallegatte et al.  
103 2016). Fortunately, recent studies have provided novel frameworks to rigorously quantify welfare  
104 impacts of disasters. For example, Walsh and Hallegatte (2019) employed agent-based modeling  
105 of consumption changes at the household level to quantify impacts of historical disasters in the  
106 Philippines; this study finds that Filipinos in the bottom income quintile experience 9% of the  
107 asset losses from these events but 31% of the wellbeing losses. Further work is needed to estimate  
108 wellbeing impacts of disasters in a changing climate.

109 In this study, we focus on TC risk assessment for the Philippines largely because this country  
110 experiences particularly high risks from these events. About 70% of Western North Pacific  
111 typhoons form in or enter the region directly surrounding the Philippines (Corporal-Lodangco  
112 and Leslie 2017). The more active period for TCs is June through December, during which time  
113 the median number of Philippines landfalls is six (Corporal-Lodangco and Leslie 2017). Around  
114 the Philippines, ENSO plays a dominant role in year-to-year variability of TC genesis frequency,  
115 tracks, and associated precipitation (Lyon and Camargo 2009; Corporal-Lodangco et al. 2016),  
116 and has been implicated in the formation of exceedingly strong storms (Lin et al. 2014).

117 Landfalling typhoons in the Philippines are disasters both in terms of economic impacts and  
118 fatalities (Ribera et al. 2008; Walsh and Hallegatte 2019). Recent storms have highlighted these  
119 dangers. In 2013, Typhoon Haiyan made landfall in the Philippines as a Category 5 storm, but  
120 with maximum sustained winds exceeding the threshold for Category 5 by over 18 m/s (Lin et al.  
121 2014). The extremely strong winds were accompanied by very high velocity surges and resultant  
122 flooding (Soria et al. 2016). The storm made a direct hit to Eastern Visayas, a region on the eastern

123 side of the Philippines. Haiyan is estimated to have cost the Philippines 13 billion USD (Ehrhart  
124 et al. 2014), and resulted in 6,300 known fatalities, the vast majority occurring in Eastern Visayas,  
125 with an additional 1,062 individuals missing and 28,688 injured (del Rosario). These impacts  
126 were exacerbated by large populations living along the coast in structurally vulnerable (wood or  
127 bamboo) housing (Mas et al. 2015; Eadie et al. 2020). For perspective, Hurricane Katrina resulted  
128 in 1,833 known fatalities and several hundred persons missing in the USA (Beven et al. 2008).  
129 Very recently, in December 2021, Typhoon Rai (Odette) made multiple landfalls in the Southern  
130 Philippines with an initial intensity of Category 5, causing widespread flooding. This disaster  
131 is the third costliest typhoon in Philippines history, affecting an estimated 12 million people and  
132 causing greater than 400 fatalities (OCHA 2022).

133 There is a strong need for accurate TC risk assessment in the Philippines to support disaster  
134 risk reduction and management efforts. However, assessment of TC risk in the Philippines is  
135 complicated by opposing spatial gradients of hazard and socioeconomic vulnerability (Figure 1).  
136 The northern Philippines experiences more frequent TCs than does the southern Philippines, but is  
137 also wealthier and more socioeconomically resilient, meaning better able to cope with and recover  
138 from disaster asset losses. The city of Manila and its surroundings (also called the National Capital  
139 Region or NCR), constitute by far the most populated and developed region in the Philippines.  
140 In contrast, the southern Philippines is generally poorer and less socioeconomically resilient.  
141 Socioeconomic resilience is defined here as the ratio of expected asset losses to wellbeing losses as  
142 in Walsh and Hallegatte (2020). These opposing patterns of hazard and resilience pose a dilemma  
143 for the Philippines itself and international agencies (such as the World Bank) aiming to distribute  
144 aid for disaster risk reduction. Should this aid focus on the northern Philippines, where exposure  
145 and hazards, and in turn asset losses, are greatest, or on the southern Philippines, which is more  
146 vulnerable and where the human wellbeing losses may be greatest? To answer this question requires

147 rigorous TC risk assessment that accurately models differences in losses across the Philippines,  
148 and, ultimately, consideration of losses across the income distribution.

149 The primary goal of the present work is to produce and validate an open-source TC risk model for  
150 the Philippines. To do so requires the development of layers for hazard, exposure, and vulnerability  
151 using methods based on publicly available data. Here we detail the development of this model. We  
152 focus on sensitivity of the results to vulnerability, as vulnerability is the component of the model  
153 that is least constrained by observational data. In particular, we demonstrate that using vulnerability  
154 that varies by region substantially improves the accuracy of TC risk estimates compared to prior  
155 country-scale analyses. We develop layers for vulnerability and exposure to combine with TC  
156 tracks from the Columbia tropical cyclone Hazard model (CHAZ), as well as with those from  
157 historical observations. CHAZ is a statistical-dynamical tropical cyclone model that can generate  
158 many physically plausible synthetic TCs based on background environmental conditions, allowing  
159 evaluation of TC risks out to longer return periods than are available from the historical record  
160 alone (Lee et al. 2018). The performance of CHAZ is comparable to that of other stochastic TC  
161 hazard models, including in the West Pacific (Meiler et al. 2022). For exposure, we employ an  
162 existing global dataset of asset value called LitPop that depends on population and nightlights  
163 data (Eberenz et al. 2020b). Finally, for vulnerability we fit parameters for an existing vulnerability  
164 function (Emanuel 2011) at the regional level by combining information on damages and wind  
165 swaths for historical TCs with data on household construction materials. In the Philippines “region”  
166 is the name for a particular administrative division; the country is divided into 17 regions (shown  
167 in center panel of Figure 1), which are further subdivided into 81 provinces. For some results,  
168 we focus on two regions as contrasting examples: 1) the National Capital Region (NCR), which  
169 contains Manila and is highly urbanized, and 2) Eastern Visayas, a relatively less affluent region  
170 that was directly impacted by Haiyan.

171 While we focus on the Philippines, the second goal of the paper is to develop a methodology  
172 that can be employed more broadly. CHAZ is global, as is LitPop, and the approach we take to  
173 vulnerability can also be applied elsewhere. While the model we develop here can be used as a  
174 stand-alone model for the Philippines, we also view it as a pilot study for the development of a  
175 global, open-source tropical cyclone risk model based on CHAZ.

176 The rest of this paper is structured as follows. Section 2 describes the methods and datasets  
177 used in this work. Section 3 shows the sensitivity of risk estimates to different assumptions about  
178 vulnerability. Section 4 applies this risk model to create TC risk estimates for the Philippines based  
179 on CHAZ. Finally, Section 5 ends this paper with a summary and conclusions.

## 180 **2. Methods**

181 Our workflow combines hazard, vulnerability, and exposure to calculate asset losses from TCs  
182 in the Philippines (Figure 2), and validates those asset losses against observations from historical  
183 storms. We describe the basic methods we use to determine each risk component separately here,  
184 and discuss vulnerability further in the next section.

### 185 *a. Hazard*

186 We make the simplifying assumption that total TC losses can be modeled as a function of  
187 wind speed. In reality, TCs cause losses through a number of different additional sub-perils  
188 associated with these events including intense rainfall, storm surge, and their associated flooding  
189 and landslides (Cinco et al. 2016). Rainfall and storm surge are only indirectly and loosely related  
190 to wind speed; for example, some relatively weak but slow moving storms can result in large  
191 amounts of rainfall (Sato and Nakasu 2011). However, due to additional complexities involved

192 in modeling rainfall and storm surge, wind speed is often used as a first order estimate of TC  
193 hazard (Eberenz et al. 2020a; Emanuel 2011).

194 We use two different types of TC track data. The first comprises historical TC tracks from  
195 the International Best Track Archive for Climate Stewardship (IBTrACS, v04r00). This version  
196 includes data from a number of different meteorological agencies across the world (Knapp et al.  
197 2010). Given that multiple agencies may provide track and intensity data for a particular storm,  
198 we choose to examine Western North Pacific track data from only the Joint Typhoon Warning  
199 Center (JTWC). Philippines-landfalling storms recorded in this dataset span the year 1945 to  
200 the present. The second data source consists of synthetic tracks from CHAZ, specifically those  
201 produced using environmental fields from the ERA-Interim reanalysis (Dee et al. 2011; Lee et al.  
202 2018). Both the historical and CHAZ tracks are available at 6-hourly temporal resolution. We  
203 extract the salient information from these tracks (latitude, longitude, maximum sustained wind  
204 speed) and linearly interpolate them to a 15-min temporal resolution. We use tracks that make a  
205 landfall in the Philippines, determined by the intersection of these 15-min resolution track points  
206 with a 5 arc-minute resolution land mask of this country. In IBTrACS, there are 480 historical  
207 Philippines-landfalling tropical cyclones. Downscaled from ERA-Interim, CHAZ generated in  
208 total 94,500 synthetic storms making landfall in the Philippines. This number includes 3178 storm  
209 tracks and each track has roughly 30 stochastically generated intensification trajectories (Lee et al.  
210 2016, 2018). For each of these landfalling storms, we use data extending from one day before the  
211 first landfall to one day after the last landfall in the Philippines for our risk analysis. Samples of  
212 landfalling TC tracks from IBTrACS and CHAZ are shown in Figure 3. Across the two sets of TCs,  
213 locations of landfall and distribution of intensities at first landfall are similar. However, CHAZ  
214 synthetic TCs do not last as long after passing through the Philippines as IBTrACS observed TCs,  
215 and are directed more southward.

216 A TC track consists of a set of points defining a one-dimensional curve in time and space, with  
217 the wind represented by a single number, the maximum sustained wind speed. It is necessary to  
218 generate two-dimensional wind swaths at each point along the track, in order to use those winds,  
219 together with spatially varying exposure and vulnerability data, to model damage. Swaths should  
220 account for the variation of wind speed from the center of the storm, and some asymmetries typical  
221 in TCs. To do this, we employ an approach based on previously published parametric wind models,  
222 described below and summarized in Figure 4. An important input to this modeling approach is  
223 the radius of maximum wind (RMW). In IBTrACS, observed estimates of RMW are available  
224 for some but not all storms. As a result, we estimate RMW using the empirically-derived Knaff  
225 et al. (2015) formula, in which the predicted RMW depends on latitude and maximum sustained  
226 wind speed. This formula was developed using data from the North Atlantic basin, where storms  
227 typically do not reach intensities as high as those in the Western North Pacific basin. A side effect  
228 of this difference is that the formula produces physically unreasonable RMW values (extremely  
229 small or negative) for the strongest storms observed around the Philippines. To compensate for  
230 this issue, any RMW values predicted by the formula to be less than 20 km are overridden to be 20  
231 km, which is on the lower end of the observed RMW distribution, similar to what is seen for high  
232 intensity storms (Hsu and Yan 1998).

233 Once we have calculated an RMW for each storm at each 15-minute time step, we can determine  
234 an associated radial profile of the azimuthal wind (Figure 4). Various parametric TC wind profile  
235 models exist (Chavas et al. 2015; Willoughby et al. 2006; Holland 1980); in all of them, azimuthal  
236 wind speed increases with radius from the eye of the storm until the RMW, at which value it begins  
237 to decrease with radius. We elect to use Willoughby et al. (2006), as it performs comparably well  
238 or slightly better than other wind profile models when compared to satellite-based observations of

hurricane wind fields (Yang et al. 2022). Inputs to this model are RMW, maximum sustained wind speed, and latitude, and the shape is determined by an empirically-fit double exponential profile.

The next step is to convert the one-dimensional radial profiles to two-dimensional wind swaths on a latitude-longitude grid. As we do this, we add a representation of asymmetry due to the translation of the storm along its track, which accelerates winds on the side of the storm where the rotating flow around the storm is in the same direction of the track, and decelerates them on the opposite side (Klotz and Jiang 2017; Uhlhorn et al. 2014). We first construct a  $0.1^\circ \times 0.1^\circ$  rectilinear grid spanning the Philippines. We then determine the track translation speed ( $V$ ) and track direction ( $\Theta$ ) from a forward difference of the time step of interest and the subsequent time step. The azimuthal velocity at each grid point imposed by the translation of the storm can then be calculated as follows:

$$\theta_{i,j} = \arctan2((y_{i,j} - Y), (x_{i,j} - X)) - \Theta$$

$$v_{t(i,j)} = -V * \cos(\pi/2 - \theta_{i,j}),$$

where  $X$  and  $Y$  are the longitude and latitude locations of the storm center,  $x$  and  $y$  are the longitude and latitude values for each point  $(i, j)$  on the grid,  $\theta$  is the angle relative to the track direction at each location  $(i, j)$  on the grid, and  $v_t$  is the imposed tangential velocity from the storm translation at each point  $(i, j)$  on the grid.

Applying a large asymmetry correction far from the storm center can result in winds increasing with radius in some directions, a feature we view as unrealistic. Thus, we modulate  $v_t$  based on distance from the storm center before applying it to the wind field:

$$\alpha_{i,j}[r_{i,j} \geq 1] = e^{-0.314 - 0.042r_{i,j}}$$

$$\alpha_{i,j}[r_{i,j} < 1] = 0.3r_{i,j} + 0.4$$

$$v_a(i,j) = \alpha_{i,j} * v_{t(i,j)},$$

262 where  $r$  is the radius from the center of the storm in kilometers normalized by the RMW (so  
263  $r = 1$  at the RMW), and  $\alpha$  is the factor modulating the asymmetry correction, and  $v_a$  is the  
264 asymmetry correction.  $\alpha$  is designed assuming that the impact of the storm motion on the  
265 symmetric background wind is reduced with radius. The above equation gives us maximum  
266 asymmetries imposed by translation speed at the RMW with  $\alpha = 0.7$  that gradually decrease to 0.3  
267 outward. The values of  $\alpha$  are within a rough range of the estimated values of storm translation to  
268 surface background wind reduction factor shown in Lin and Chavas (2012).

269 The final wind field is determined by re-gridding the Willoughby et al. (2006) radial wind profile  
270 to the latitude-longitude grid and adding the asymmetry correction ( $v_{a(i,j)}$ ). To this end, to ensure  
271 the maximum wind speed remains unchanged, we input to the wind profile calculation the maximum  
272 sustained wind speed minus the maximum asymmetry correction ( $\max(v_a) = 0.7 * \max(v_t)$ ). Once  
273 a wind field is determined for each 15-minute time step of a given storm, the final wind swath  
274 to be used in loss calculations is obtained by taking the maximum of all the wind fields across  
275 time at each latitude-longitude grid point. Examples of resulting wind swaths for nine of the most  
276 destructive historical storms in the Philippines are shown in Figure 4.

277 Here we presented a relatively simple construction of two-dimensional wind swaths that captures  
278 storm wind at first-order, and allows efficient generation of wind maps for large numbers of synthetic  
279 storms. However, there are a variety of ways in which this construction could be improved. For  
280 example, one can use a more sophisticated method in estimating RMW (Chavas and Knaff 2022) and  
281 in adding in asymmetries (Lin and Chavas 2012; Chang et al. 2020; Yang et al. 2022). Additionally,  
282 following landfall, another significant source of asymmetry in the wind field is the roughness of  
283 the land surface (e.g. from buildings, plants, and topography), which generally decelerates wind  
284 speeds. For our initial model described here, we neglect this roughness effect. This will lead to  
285 overestimates of the wind over land, but we view this as an acceptable compromise for the level

286 of analysis we conduct here, particularly because the vulnerability curves are calibrated to these  
287 winds. Roughness will be incorporated in future versions of the model.

### 288 *b. Exposure*

289 We represent exposure via a global dataset of assets in USD across space developed by Eberenz  
290 et al. (2020b). This dataset, called LitPop, is constructed by disaggregating 2014 national total  
291 asset value across space proportionally to population density and nightlights data. The national  
292 total asset value data used is the World Bank’s produced capital stock, which represents the value of  
293 manufactured or built assets in each country, not including the value of agricultural products (World  
294 Bank 2021). The nightlights data used is NASA’s Black Marble nighttime lights (Román et al.  
295 2018), and the population data used is the Gridded Population of the World (Doxsey-Whitfield et al.  
296 2015). Validating by disaggregating national GDP and comparing to regional GDP estimates in  
297 14 countries, Eberenz et al. (2020b) finds that disaggregating proportionally to  $Lit^1 Pop^1$  (where  
298 *Lit* is the nightlights data and *Pop* is the population data) likely provides the best estimate of  
299 asset distribution. It is worth noting that the validation exercise was performed in a set of 14  
300 countries that did not include the Philippines. An improved Philippines-specific dataset might be  
301 constructed by fitting this dataset for the Philippines, and perhaps considering the distribution of  
302 agricultural products across space. But we expect that the existing dataset provides a reasonable  
303 enough estimate of asset distribution for this initial risk model. In the Philippines, LitPop shows by  
304 far the highest asset density in and around Manila, with more minor hot spots of asset concentration  
305 in other major cities (Figure 5).

306 LitPop is available at a relatively high 30 arcsec resolution, which is equivalent to the resolution  
307 of the underlying population data. To allow the wind hazard to interact with exposure, we bilinearly

308 interpolate the  $0.1^\circ \times 0.1^\circ$  wind swaths to the higher resolution of the LitPop data. This is done to  
 309 leverage the spatial detail in the exposure dataset.

### 310 *c. Vulnerability*

311 Vulnerability is the propensity of exposed value to be destroyed in the face of a geophysical  
 312 hazard. In the context of our model, vulnerability converts a given wind speed to percentage of  
 313 assets destroyed. Intuitively, at low to moderate wind speeds — i.e., those that are commonly  
 314 experienced in the absence of a tropical cyclone — no damages should occur, and at high wind  
 315 speeds damages should increase until they saturate at 100% of exposed value. There are a few  
 316 different functional forms for TC wind-related vulnerability (called impact functions, vulnerability  
 317 curves, or damage functions) that have been proposed. Here we use the functional form presented  
 318 in Emanuel (2011), which is structured as follows:

$$319 \quad f = \frac{v_n^3}{1 + v_n^3} \quad (1)$$

$$320 \quad v_n = \frac{\max[(V - V_{thresh}), 0]}{V_{half} - V_{thresh}}, \quad (2)$$

321 where  $f$  is the fraction of the asset value lost,  $V$  is the wind speed,  $V_{thresh}$  is the wind speed at and  
 322 below which no damage occurs, and  $V_{half}$  is the wind speed at which half the asset value is lost  
 323 (Figure 6). The third power of wind speed in Equation 1 is based on physical arguments (Emanuel  
 324 2005) and empirical analysis, i.e. regression against historical losses in the USA (Strobl 2011).  
 325 In the function shown in Equation 2, the parameters  $V_{thresh}$  and  $V_{half}$  determine vulnerability—  
 326 lower values of these parameters correspond to higher vulnerability.  $V_{thresh}$  is necessarily always  
 327 lower than  $V_{half}$ .

328 The vulnerability function above was developed to represent damage from extreme wind, but  
 329 has been used to predict total TC-related damages in various applications. Most relevant to this

330 study, Eberenz et al. (2020a) (hereafter, “ELB21”) fit country-wide impact functions to simulate  
331 total historical TC damages in different countries, including the Philippines. In this study, the  
332 values of  $V_{half}$  are varied to optimally simulate total damages, while  $V_{thresh}$  is kept constant at  
333  $25.7ms^{-1}$  (50kts), an approach that has been used and to some degree supported in other studies.  
334 For example, in Emanuel (2011) this  $25.7ms^{-1}$   $V_{thresh}$  value was proposed for the USA, while  
335 the value of  $V_{half}$  varied in order to represent different vulnerability levels, and this same  $V_{thresh}$   
336 value is somewhat consistent with structural vulnerability curves for wind used in the Hazus risk  
337 modeling framework (Vickery et al. 2006b). This approach of varying  $V_{half}$  but not  $V_{thresh}$  has  
338 also been shown to reasonably simulate losses in China (Elliott et al. 2015). Since there is rather  
339 limited justification of this  $V_{thresh}$  value when using wind as a proxy for all damages, and it is  
340 plausible that lower  $V_{thresh}$  values may be justified to the extent that non-wind hazards (such as  
341 flooding) are being implicitly represented, we examine sensitivity of our risk results to both  $V_{half}$   
342 and  $V_{thresh}$ .

343 Our process for fitting this vulnerability function for the Philippines is discussed in more detail  
344 in Section 3. A dataset we use in this fitting process is the Family Income and Expenditure Survey  
345 (FIES) for the Philippines. FIES is conducted by the Filipino government’s National Statistics  
346 Office, and is a key tool for poverty quantification (Ericta and Fabian 2009). It surveys tens  
347 of thousands of households in the Philippines on diverse and detailed aspects of their incomes,  
348 spending, and saving. Particularly relevant here, it also includes information on their dwellings.  
349 This survey is completed every three years. We employ 2015 data on dwelling construction  
350 materials (Bersales 2017). The FIES categorizes roof and wall construction materials into seven  
351 different categories, which can roughly be ordered from weakest to strongest. As discussed below,  
352 we employ this data as a proxy for TC structural vulnerability.

353 *d. Reported Damage Data*

354 To develop and validate our risk model, we compare our results to estimates of historical losses  
355 from real TCs that have affected the Philippines. For this purpose, we use the EM-DAT database,  
356 which aggregates data on a wide range of disasters (Guha-Sapir et al.). EM-DAT includes disasters  
357 from 1900 to the present that meet one of the following criteria: 10 or more people dead, 100  
358 or more people affected, the declaration of a state of emergency, and/or a call for international  
359 assistance. Sources of data included in EM-DAT vary, but priority is given to information from UN  
360 agencies, governments, and the International Federation of Red Cross and Red Crescent Societies.  
361 From EM-DAT, we select only data entries for storms affecting the Philippines, and make use of  
362 the start date, end date, and total damages (in USD) for each storm. We retain storms that have  
363 damage estimates, start and end dates, and are not labelled as convective or extra-tropical events  
364 (260 events total). While tropical cyclones are convective in nature, all events with the convective  
365 label in Philippines EM-DAT are either tornados or related to frontal systems, hence their exclusion  
366 from our analysis. 245 of the 260 included events are labeled as TCs. The event names of the  
367 remaining 15 indicate that these are tropical depressions or tropical storms— we also include these  
368 in our analysis, as they were TCs but just did not have typhoon-intensity at the time of landfall in  
369 the Philippines. The timing of these events spans 1952 to the present (Figure 7). Their associated  
370 losses span many orders of magnitude, with the smallest loss for an individual TC event being 5000  
371 USD, and the greatest loss being 10 billion USD, caused by Typhoon Haiyan.

372 The number of events included in the dataset also increases over time— this may result from  
373 changes in observing practices or actual increases in TC risk caused by population growth and  
374 development and/or changes in TC characteristics (in particular TC intensity) due to anthropogenic  
375 climate change (Knutson et al. 2020). Here, we evaluate the model by comparing simulated

376 damages to those in EM-DAT event-by-event, without explicitly considering when each event  
377 occurred, so any changes in observing practices are effectively random errors for our purpose. The  
378 possible effects of such changes would have to be considered more explicitly if one wished to study  
379 temporal trends in damage.

380 *e. Comparison between Reported and Simulated Damages*

381 To reasonably compare EM-DAT with our simulated damages we need to account for change  
382 in assets over time and inflation. However, the LitPop dataset uses asset data from 2014, while  
383 the damage values in EM-DAT should be compared to asset values at the time the event occurred.  
384 Therefore, in order to reasonably compare simulated and observed damages, we first normalize  
385 the observed damages to 2014 values via the Penn World Tables' (version 10.0) quantification of  
386 Philippines capital stock, which is closely related to total asset value (Feenstra et al. 2015) and  
387 provided in units of constant 2017 national prices in USD. Specifically, we follow a procedure  
388 similar to that in ELB21:

$$389 \quad \text{NRD}_E = \text{RD}_E \frac{\text{CS}_{2014}}{\text{CS}_y},$$

390  
391 where E represents a particular event, y is the year the event occurs, RD is the raw reported  
392 damages, NRD is normalized reported damages, and CS is capital stock. For the rest of this paper,  
393 "reported damages" refers to damages normalized this way.

394 EM-DAT presents damages in entire country totals. For some events, additional information  
395 is provided specifying the region affected, but the lack of consistency in this information makes  
396 it difficult to employ in our analysis. As such, in validating simulated damages against reported  
397 damages, we always first sum all simulated damages across the Philippines.

398 To match reported damages with corresponding simulated damages, we employ the dates of the  
399 events from EM-DAT and IBTrACS. Since multiple storms can share some dates of occurrence,  
400 we match a reported damage entry and simulated damages when the number of days of overlap is  
401 maximized compared to any other possible matches. Using this method results in 134 unambiguous  
402 matches. There were some ambiguous matches that required special considerations. First, two  
403 sets of events share very similar dates—1995’s typhoons Angela (Pepang) and Zack (Rosing), and  
404 2016’s typhoons Sarika (Karen) and Haima (Laiwin), where the first name is given by the Japan  
405 Meteorological Agency (JMA) and the second in parentheses is given locally by the Philippine  
406 Atmospheric, Geophysical, and Astronomical Services Administration (PAGASA), only when  
407 storms enter into their area of responsibility. For these pairs of TCs, matching was reconciled  
408 via looking up additional information about storm path and precise landfall date. There is also  
409 ambiguity for Typhoon Faye (Norming) in 1982 — two entries exist in EM-DAT for this event (one  
410 under Typhoon Faye, the name given by JMA, and one under Typhoon Norming, the local name  
411 given by PAGASA). These two entries have different damage estimates which appear to correspond  
412 to different landfalls of this one storm. We add these two damage estimates together to create one  
413 reported estimate for the typhoon that is comparable to the entire simulated event. Many storms  
414 are excluded because there is an IBTrACS track but no overlapping EM-DAT damage event, or  
415 vice versa. Altogether, this process results in matches for 139 events.

416 We use a few different metrics to compare reported and simulated damages. Three are standard  
417 metrics of correlation: Pearson’s  $r$ , Kendall’s  $\tau$ , and Spearman’s  $r$ . Pearson’s  $r$  measures the  
418 linear correlation between two datasets, whereas Kendall’s  $\tau$  and Spearman’s  $r$  are both non-  
419 parametric, rank-based correlation coefficients— they assess the extent to which one dataset is  
420 a monotonic function of the other. For all three of these metrics, model performance is better  
421 when the correlation is closer to 1. The two additional metrics are drawn from ELB21, and reflect

422 distinct needs in developing a TC risk model. The first metric is the total damage ratio (TDR), and  
423 is quantified as:

$$424 \quad \text{TDR} = \frac{\sum_{E=1}^N \text{SD}_E}{\sum_{E=1}^N \text{NRD}_E},$$

425

426 where  $E$  from 1 to  $N$  spans all the relevant historical TC events, NRD is the normalized reported  
427 damages, and SD is our model's simulated damages. A TDR of 1 is optimal. TDR reflects the  
428 ability of our risk model to simulate total damages across all events, and is dominated by the events  
429 that cause the greatest asset losses (e.g., Haiyan). However, as discussed further in Section 3, lack  
430 of skill in simulating more moderate events can be masked by TDR. To better assess skill across a  
431 range of events, ELB21 also introduces a metric called root-mean-squared fraction (RMSF), which  
432 is quantified as:

$$433 \quad \text{RMSF} = \exp\left(\sqrt{\frac{1}{N} \sum_{E=1}^N [\ln(\text{EDR}_E)]^2}\right),$$

434

435 where EDR stands for "event damage ratio" and is defined as  $\text{SD}_E/\text{NRD}_E$  for any given event.  
436 RMSF weighs errors proportionally to event magnitude, so that a 50% error (for example) is equally  
437 important whether it is 50% of a small loss or a large one. Values of RMSF closer to one represent  
438 lower model errors. TDR and RMSF reflect different considerations relevant to development of  
439 a TC risk model. Ideally a model would perform well for both metrics, but in general (and in  
440 our results below) there are trade-offs such that prioritizing one versus the other implies different  
441 modeling choices.

### 3. Development of the Vulnerability Layer

In this section, we estimate vulnerability across space in the Philippines, which we call a “vulnerability layer” to be combined with hazard and exposure to estimate Philippines TC risk. In developing a vulnerability layer, our general approach is to determine which vulnerability parameter values result in the best match between reported damages and simulated damages for historical TCs. As mentioned above, we only consider TCs that make landfall in the Philippines (excluding near misses), and are included in EM-DAT. Fitting vulnerability to damages as described here is primarily an empirical approach, though we note that the Emanuel (2011) vulnerability curve functional form we employ is also informed by the physics of wind-driven damage. Below we describe a couple of specific methods for fitting vulnerability in the Philippines with varying levels of spatial complexity.

#### *a. National Fit*

We initially apply the same vulnerability curve for all locations in the Philippines. This is similar to the approach employed in ELB21, who notably found very different values for  $V_{half}$  in the Philippines depending on whether TDR or RMSF was optimized, which were  $85.7ms^{-1}$  and  $188.4ms^{-1}$  respectively. Using these  $V_{half}$  values and the  $V_{thresh}$  value used in ELB21 ( $25.7ms^{-1}$ ) as a starting point, we test the sensitivity of simulated damages to  $V_{half}$  and  $V_{thresh}$ . Specifically, we evaluate simulated damages for  $V_{half}$  every  $10ms^{-1}$  between 50 and  $200ms^{-1}$ , and for  $V_{thresh}$  every  $5ms^{-1}$  between 15 and  $35ms^{-1}$ . For each combination of these parameter values, we calculate the various correlation metrics described in Section 2 comparing simulated versus reported damages (Figure 8). In this analysis, the parameter values for vulnerability are deemed more optimal when Pearson’s  $r$ , Kendall’s  $\tau$ , and Spearman’s  $r$  are closer to 1, TDR is closer to 1 (equivalent to  $\ln(\text{TDR})$  closer to 0), and RMSF is minimized.

465 This sensitivity analysis highlights the difficulty of confidently fitting a single vulnerability curve  
466 for the Philippines. Depending on the correlation metric examined, very different parameter values  
467 are found to be optimal. Not only that, but the structure of the dependence of the correlation  
468 metrics on the vulnerability parameters varies substantially. Pearson  $r$  is optimized for the highest  
469 values of  $V_{half}$  and  $V_{thresh}$ . Kendall  $\tau$  and Spearman  $r$ , which are both rank-based, non-parametric  
470 correlation metrics, exhibit the strongest dependence on  $V_{thresh}$ , and are optimized for  $V_{thresh}$  equal  
471 to  $30ms^{-1}$ . TDR is optimized along a diagonal from high values of  $V_{thresh}$  and low values of  
472  $V_{half}$  to low values of  $V_{thresh}$  and high values of  $V_{half}$ . Finally, RMSF is generally optimized for  
473 somewhat lower values of both parameters, and favors  $V_{thresh}$  equal to  $20ms^{-1}$ .

474 For TDR and RMSF, the results of our analysis are qualitatively similar to those of ELB21, though  
475 quantitatively different. If we hold  $V_{thresh}$  constant at  $25ms^{-1}$ , as ELB21 does, we find TDR is  
476 optimized at  $V_{half}$  equal to  $150ms^{-1}$  and RMSF is optimized at  $V_{half}$  equal to  $80ms^{-1}$ . These values  
477 are both lower than the analogous fits in ELB21 ( $188.4ms^{-1}$  and  $84.7ms^{-1}$ , respectively). This  
478 difference could perhaps be a consequence of ELB21 excluding storms where reported damages  
479 are positive but simulated damages are zero from their analysis, whereas we include such storms.  
480 However, additional differences may lie in the time span of the TC and damage data used, the wind  
481 field modeling, and the method of matching simulated damages and reported damages.

482 For the rest of the paper, we simplify our vulnerability fitting procedure in a few ways for  
483 parsimony and consistency with prior work. First, we focus on optimizing TDR and RMSF, which  
484 we believe are more intuitive to interpret than the other correlation metrics for emergency planning  
485 and preparedness. Second, rather than continuing to fit  $V_{thresh}$  and  $V_{half}$ , we hold  $V_{thresh}$  constant  
486 at  $25ms^{-1}$  (same value as ELB21) and vary only  $V_{half}$ . As measured by TDR and RMSF, the  
487 degree of agreement with observed damages can be fit to some extent either by  $V_{thresh}$  or  $V_{half}$   
488 (Figure 8d,e); focusing on  $V_{half}$  seems a reasonable simplifying assumption, especially as we have

489 a somewhat stronger *a priori* constraint on  $V_{thresh}$  (that is, that it should be somewhere near the low  
490 end of the maximum sustained wind speeds found in tropical storms). However, we emphasize that  
491 the sensitivity analysis shown in Figure 8 cannot clearly exclude values of  $V_{thresh}$  greater or lower  
492 than  $25ms^{-1}$ . Unlike prior work which has stated that  $V_{thresh}$  is relatively well-constrained to be  
493 around  $25ms^{-1}$  (Emanuel 2011; Elliott et al. 2015), our analysis suggests further examination of  
494 appropriate  $V_{thresh}$  values is warranted, particularly in contexts where, as here, wind is being used  
495 as a proxy for all damages, rather than modeling only damages directly caused by wind.

496 Figure 9 plots reported against simulated damages for historical TCs, with the vulnerability  
497 parameter set to the optimal RMSF fit when holding  $V_{thresh}$  constant at  $25ms^{-1}$  ( $V_{half} = 80ms^{-1}$ ).  
498 When RMSF is minimized, TDR is 9.28— meaning total simulated damages are about  $9\times$  greater  
499 than those reported. This suggests a significant trade-off between capturing the damages for  
500 individual storms and across all storms when applying one vulnerability curve for the entire  
501 Philippines. To better understand the cause of this overestimation of total damages, we assessed  
502 possible commonalities among outliers. We found that storms passing through the large urban  
503 capital region, including Manila, by and large exhibited overestimated simulated damages. This  
504 is shown in Figure 9a by the blue circled values climbing the y-axis (simulated damages) for very  
505 low reported damages values, in Figure 9b by all the blue circled values lying above the black  
506 one-to-one line, and in Figure 9c by storms that pass through Manila disproportionately exhibiting  
507 high event damage ratios. Figure 9c is very similar to and inspired by Figure 7 in ELB21, though  
508 we find more storms with event damage ratios less than 0.1 as we include storms where simulated  
509 damages are 0.

510 These results seem to reflect the limitations of country-scale vulnerability in capturing significant  
511 urban-rural differences. Manila is much more built-up and wealthier than other regions in the  
512 Philippines, with likelier lower vulnerability (though greater exposure). As a result, when a

513 vulnerability curve fit for the entire Philippines is employed to calculate damages for a storm  
514 passing through Manila, damages are overestimated. Our hypothesis is that developing a more  
515 spatially detailed map of vulnerability in the Philippines would better capture these urban-rural  
516 differences, and allow more accurate simulation of damages for individual storms (i.e. lower  
517 RMSF) and across all storms (i.e. TDR closer to 1).

### 518 *b. Regional Fit*

519 Motivated by the results above, we develop a vulnerability layer with spatial variability in the  
520 vulnerability parameters. To capture a very high level of spatial detail, one might match buildings  
521 across the Philippines with building-type specific vulnerability curves similar to the methodology  
522 used for the US in FEMA’s Hazus (Vickery et al. 2006b). However, this approach requires a detailed  
523 map of building types across the Philippines, which we lack. Instead, we take an intermediate  
524 approach between a single empirically-derived vulnerability curve for all the Philippines (the  
525 approach used in the previous section) and a building-level map of structural vulnerability to  
526 develop a region-scale TC vulnerability layer for the Philippines.

527 Our first step is to fit  $V_{half}$  for each region in the Philippines that has historically been damaged  
528 by TCs. A challenge here is that EM-DAT only provides nationally aggregated damage estimates.  
529 In lieu of region-level damage data, we fit  $V_{half}$  for each region based on the subset of historical  
530 storms that result in positive simulated asset losses for that region. Given the limitations of EM-  
531 DAT we also compare the national sum of reported damages to simulated damages, but just for  
532 the subset of storms affecting a given region. The assumption here is that even though the damage  
533 estimate for any given storm may be affected by neighboring regions impacted by the same TC, in  
534 aggregate across all historical storms this subset should reflect the TC risk for the region of interest.  
535 We then determine the  $V_{half}$  values that minimize RMSF for storms affecting each region. For

536 most regions,  $V_{half}$  ranges from  $60 - 120ms^{-1}$ . Manila, as predicted, exhibits lower vulnerability  
537 than any other region, with an optimal  $V_{half}$  equal to  $180ms^{-1}$ .

538 Because some regions of the Philippines have been affected by very few storms in the historical  
539 record, however, it is highly uncertain or impossible to fit  $V_{half}$  using the method described above  
540 for every region. For example, the Autonomous Region in Muslim Mindanao (ARMM) has  
541 experienced zero recorded landfalling storms according to our analysis of IBTrACS. To create a  
542 vulnerability map that is consistent across the Philippines, and also lend further confidence to our  
543 vulnerability quantification, we employ on-the-ground data about structural vulnerability included  
544 in the FIES. The FIES surveys a sample of households and groups them by region, making it  
545 possible to derive region-scale information. While the FIES includes information on both roof and  
546 wall construction materials, we focus on the roof materials, as most TC structural damage occurs  
547 through damage to the roof allowing rain to enter a building (Rowe 2021). The roof materials listed  
548 in the FIES dataset fall into seven categories (Figure 10). Most roofs are categorized as “strong  
549 material (galvanized, iron, al[uminum], tile, concrete, brick, stone, asbestos)” or “light material  
550 (cogon, nipa, anahaw)”. Cogon, nipa, and anahaw are plant materials used to make straw thatch  
551 roofs. We use the ratio of strong to light roof materials as a proxy for structural vulnerability  
552 (Figure 11). As might be expected, the region of Manila has the highest proportion of strong to  
553 light roofs, whereas a more rural and impoverished region such as Eastern Visayas has a much  
554 lower proportion of strong to light roofs.

555 We hypothesize that the proportion of strong to light roofs influences TC vulnerability and  
556 should positively correlate with the  $V_{half}$  value fit in different regions. Indeed, we find a positive  
557 association between these two quantities (Figure 12a; NCR is the top-right point in the plot).  
558 This association likely reflects the direct impact of roof strength on TC damages, as well as other  
559 socioeconomic factors such as income and extent of the social safety net, which partially correlate

560 with construction quality and influence disaster outcomes. We linearly regress the proportion  
561 of strong to light roofs against  $V_{half}$ , and use the resulting regression coefficients and regional  
562 values of the roof proportion to calculate a final  $V_{half}$  value for each region (Figure 12a). The  
563 resulting map of vulnerability (represented by  $V_{half}$  values; Figure 12b) is similar to the map of  
564 socioeconomic resilience shown in Figure 1: vulnerability is higher in the south, and lower in the  
565 north, especially close to Manila.

566 We employ this map of regional vulnerability to recalculate simulated damages for historical  
567 storms making landfall in the Philippines and compare to reported damages from EM-DAT. The  
568 results of this analysis are shown in Figures 13 and 14. Compared to the nationally fit vulnerability  
569 curves minimizing RMSF (Figure 9), the regionally-varying vulnerability curves result in smaller  
570 RMSF (81 versus 92). Perhaps more striking, TDR is reduced from 9.28 to 2.02, even though TDR  
571 was not explicitly optimized for. For individual regions in the Philippines, TDR calculated for the  
572 subset of storms affecting each region is much improved as well. With a single national vulnerability  
573 curve, northern regions reach TDR values above 20 (Figure 14). In contrast, considering regionally  
574 varying vulnerability curves, leads to TDR values below 10 across the Philippines, and in most  
575 cases quite close to 1.

576 While key aspects of the simulated damages compare better to reported estimates with spatially  
577 varying vulnerability, as described above, others do not. In particular, with both versions of the  
578 vulnerability layer (national and regional) there are many storms with substantial reported damages  
579 that have zero simulated damages (Figure 13b). This error likely represents a structural limitation  
580 of our risk model. Here we use wind as a proxy for all TC-related damages. However, other hazards  
581 associated with TCs (storm surge, flooding due to rainfall, landslides) may occur at relatively low  
582 wind speeds (e.g. lower than the  $V_{thresh}$  value of  $25ms^{-1}$  used in the vulnerability curve), and  
583 result in damages which our model does not capture.

584 As an illustrative example, simulated damages from typhoons Haiyan (Yolanda) and Ketsana  
585 (Ondoy) are shown in Figure 15. Our model simulates no damages resulting from Ketsana, though it  
586 actually produced damages of 240 million USD according to EM-DAT. This appears to be because  
587 Ketsana was a relatively weak storm (tropical storm intensity) in terms of wind speed when it  
588 affected the Philippines, with damages dominated by extreme rainfall and flash flooding (Sato and  
589 Nakasu 2011), processes our model does not represent in any explicit way. In contrast, our model  
590 does simulate billions of USD worth of damages from Typhoon Haiyan, though it underestimates  
591 those damages by a factor of 5. This may reflect the lack of explicit storm surge in our model, as a  
592 large fraction of the damages caused by Haiyan resulted from storm surge (Lagmay et al. 2015).

#### 593 **4. Return Periods of TC Risk in the Philippines**

594 The goal of this work was to create a usable, country and regional-scale TC risk model for  
595 the Philippines. Before concluding the paper, we briefly highlight the utility of our model for  
596 estimating TC risk return periods in the Philippines.

597 In assessing TC risk for diverse aspects of emergency preparedness, from building construction  
598 standards to emergency response plans, it is useful to know the expected frequency of events of a  
599 given severity. This is typically quantified as a return period ( $1/\text{frequency}$ ) in units of years. Using  
600 our model, we can calculate return periods empirically for both wind speed and asset losses for  
601 different regions in the Philippines (examples for NCR and Eastern Visayas are shown in Figure  
602 16). The most accurate hazard input is obtained using historical TC tracks, but this allows accurate  
603 estimation only at return periods several times shorter than the length of the historical record (76  
604 years). Using our TC risk model run with CHAZ tracks allows consistent estimation of TC wind  
605 speed and asset losses out to much longer return periods. For CHAZ, we specify the duration used  
606 for frequency and return period calculation such that the regional landfall rate per year in CHAZ

607 is consistent with that of the historical record— i.e. for each region:

$$608 \quad \textit{duration}_{\text{CHAZ}} = \textit{landfalls}_{\text{CHAZ}} / (\textit{landfalls}_{\text{IBTrACS}} / \textit{duration}_{\text{IBTrACS}}),$$

609

610 which amounts to a regional-scale bias correction on the landfall rate.

611 Both the advantages and the challenges of this approach are clearly demonstrated in determining  
612 the return period for a Haiyan-like event in Eastern Visayas as shown in Figure 16. Based on the  
613 historical record, in Eastern Visayas Typhoon Haiyan has a return period of about 70-80 years  
614 (since it occurred within the bounds of a historical record of approximately that length), but is  
615 clearly an outlier and not well-constrained. In the context of the much larger sample of physically  
616 plausible TCs from CHAZ, the hazard associated with a Haiyan-like event has a return period  
617 of several thousand years, and the losses from such an event are outside the range of synthetic  
618 storms (e.g. return period greater than 10,000 years). While the larger sample of storms may  
619 more robustly constrain the return period of this event, there are important caveats to consider  
620 with this estimate. In particular, CHAZ (like any model) may have biases— in Eastern Visayas,  
621 CHAZ-based asset losses appear to be biased somewhat too low given that the historical records  
622 lies slightly above the intensity ensemble (thin red lines). While we perform some light bias  
623 correction on the regional landfall rate (as mentioned in the prior paragraph), more intensive bias  
624 corrections could be applied, such as sub-selecting more realistic CHAZ tracks. Additionally, the  
625 CHAZ simulations here used environmental variables taken from the ERA-Interim Reanalysis in  
626 the recent historical period, with all years treated the same in the return period calculation; thus  
627 any possible climate change signal would be obscured to the extent that it might render 2013 (when  
628 Haiyan occurred) different than the earlier part of the period.

## 5. Summary & Conclusions

We have described the development and application of a TC risk model for the Philippines. This model includes three layers—hazard, exposure, and vulnerability—which, when combined, allow quantification of asset losses from storms. The present study focuses on the Philippines, but the methodology could be straightforwardly applied to other countries. Hazard is represented by swaths of maximum sustained wind speeds, derived from a parametric wind field model with a simple geometric correction for TC asymmetry. Swaths can be derived from observed TC tracks (e.g. IBTrACS) or synthetically generated TC tracks, such as from CHAZ. Exposure is the existing LitPop dataset, which distributes national total asset value across each country proportional to a combination of nightlights and population data (Eberenz et al. 2020b). For vulnerability, we employ the Emanuel (2011) functional form for vulnerability. However, we run a number of tests to fit the vulnerability curve parameters ( $V_{half}$ ) to accurately simulate historical losses. This work is novel in two main ways. First, while there are other existing TC risk models, this is the first attempt to utilize the CHAZ model to quantify economic risks from TCs, opening the door for a variety of future applications. Second, we demonstrate the benefits of fitting regional (as opposed to national) vulnerability curves based on open-source economic data for TC risk analysis.

Initially, we tried fitting one vulnerability curve for the entire Philippines. Similar to results in ELB21, we find that this approach results in substantial uncertainty regarding the appropriate vulnerability curve. If the vulnerability is fit to best represent total damages (TDR close to 1), damages from TCs that pass through Manila are well simulated, while damages from other storms are underestimated. In contrast, if all storms are weighted equally in fitting vulnerability (RMSF minimized), damages from TCs that pass through Manila are substantially overestimated, and the TDR is approximately 9.

652 We hypothesized that this trade-off regarding the appropriate vulnerability curve resulted from  
653 urban-rural differences not captured by a national-scale vulnerability fit. We tried instead fitting  
654  $V_{half}$  for each region to minimize RMSF based on the subset of historical storms that affected each  
655 region. The  $V_{half}$  values from this analysis suggest that Manila indeed has the lowest vulnerability  
656 in the Philippines. These parameter values were also found to be positively correlated with a proxy  
657 of structural vulnerability based on household survey data, namely, the proportion of strong to  
658 light roofs. Regressing  $V_{half}$  against this roof strength proportion, we determined  $V_{half}$  values  
659 for each region of the Philippines, and in so doing a regional map of TC vulnerability. Applying  
660 this regional TC vulnerability layer to simulate historical Philippines storms, we find lower RMSF,  
661 TDR across the Philippines of 2, and TDR values for individual provinces much closer to 1. We  
662 conclude that regional, and especially urban versus rural, differentiation of vulnerability is critical  
663 for accurate TC risk modeling in the Philippines.

664 We hope the initial TC risk model presented here may serve as a basis for further open-source TC  
665 risk modeling. Many aspects of this model could be improved, and we highlight a few here. On the  
666 hazard front, modeling of other TC-related hazards beyond wind could allow better simulation of  
667 impacts from many storms (Lin et al. 2010, 2012; Aerts et al. 2013; Rodrigo et al. 2018). At present,  
668 our model simulates zero damages for some historical TCs that did in fact produce damage. We  
669 believe this is because these are storms dominated by rainfall and flooding— hazards that are only  
670 indirectly, and very loosely, related to wind speed. Regarding the existing wind model, capturing  
671 surface roughness could allow more accurate simulation of wind speeds, and in turn damages, over  
672 land. We expect this limitation to be much less important than the omission of flooding, however,  
673 in part because our vulnerability curves are fit to the winds we use. The regional vulnerability  
674 approach can compensate further (compared to the national fit) for the lack of roughness in our  
675 model, as vulnerability is found to be lowest in urban regions where roughness would likely be

676 decelerating surface winds to the greatest extent. The method of incorporating TC asymmetry here  
677 is also a relatively simple function of TC translation, which might be superseded in future model  
678 iterations by more advanced methods (Lin and Chavas 2012; Chang et al. 2020; Yang et al. 2022).

679 There are many areas within the vulnerability and exposure modeling that merit further devel-  
680 opment as well. First, agricultural losses could be more rigorously quantified. At present, the  
681 exposure layer includes built assets, but does not explicitly include agriculture. This may bias our  
682 results, as agricultural losses have been significant in many historical Philippines TCs (Eberenz  
683 et al. 2020a). Second, appropriate values of the vulnerability parameter  $V_{thresh}$  might be more  
684 robustly determined, particularly in countries with a wide range of different construction standards.  
685 Here we have focused primarily on fitting  $V_{half}$ , but our national vulnerability curve fitting results  
686 suggests that in some circumstances values of  $V_{thresh}$  higher or lower than that used here ( $25ms^{-1}$ ,  
687 similar with prior work) could be more accurate. This issue is perhaps particularly acute when wind  
688 is used as a proxy for all TC-related hazards, since substantial flooding can occur at relatively small  
689 wind speeds. Third, more work could be done to examine the causes of the regional variation in  
690 vulnerability. While we relate regional  $V_{thresh}$  values to a measure of the strength of roof construc-  
691 tion materials, the positive relationship between these two quantities does not necessarily reflect  
692 stronger roofs directly reducing vulnerability. Proportion of strong roofs may simply correlate  
693 with other quantities that could reduce vulnerability, such as wealth and urbanization. Indeed, in  
694 some small island communities in the Philippines, light cogon roofs are actually reported to be  
695 adaptive to tropical cyclones, as they can be tied down in high winds (Board 2019), highlighting  
696 a limitations of our focus on strong/heavy roofs to explain vulnerability. Fourth and finally, while  
697 moving from national to regional scale vulnerability significantly improved model accuracy, even  
698 higher resolution vulnerability layers (e.g. province or even building scale) may result in further  
699 improvements.

700 The current model quality encourages caution in interpreting results from such analyses, espe-  
701 cially for individual storms which could be dominated by hazards other than wind. However, in  
702 simulating aggregate damages across many storms, the present risk model exhibits significant skill.  
703 Building on the return period analysis, we hope in future work to estimate projected changes in TC  
704 risk with global warming via pairing this model with CHAZ tracks generated using environmental  
705 variables taken from climate change scenarios simulated with earth system models (Emanuel 2011;  
706 Lee et al. 2020). Such results would be relevant to both adaptation planning and financial risk  
707 modeling, which regulations increasingly require to consider climate change (Fiedler et al. 2021).

708 Despite these various limitations, the model and analysis presented here generates insights  
709 useful for all stages of disaster risk management policy dialogues. Expected asset losses are used  
710 in sovereign risk financing dialogues to define needs and insurance premiums. Simulations of  
711 extreme events are useful for assessing tail risks and compound shocks, relevant to macro-fiscal  
712 and humanitarian contingency planning. We intend to extend this model to assess TC impacts  
713 across the income distribution, which is useful for mapping and addressing vulnerabilities, and for  
714 crafting post-disaster assistance packages. All of these considerations are in flux due to differential  
715 economic and population growth throughout the Philippines, and climate change. Because of these  
716 dynamics, perhaps the most salient contribution of this work to domestic policy and international  
717 development is its open source methods and code, which increase access to resources generally  
718 reserved for wealthy countries, the reinsurance industry, and private capital.

719 *Acknowledgments.* We would like to thank Samuel Eberenz, Olivia Cabrera, Dail Rowe, Kyle  
720 Mandli, and Stephane Hallegatte for useful conversations and feedback. We also thank Qidong  
721 Yang for sharing his implementation of the Willoughby wind profile model. JWB was supported  
722 by the Lamont-Doherty Earth Observatory Postdoctoral Fellowship. CYL and SJC thank support

723 from the Vetlesen Foundation to the Lamont-Doherty Earth Observatory of Columbia University.  
724 SJC, CYL, and AHS acknowledge support from the Swiss Re Foundation.

725 *Data availability statement.* Upon acceptance, code and data supporting the analyses and figures  
726 in this manuscript will be made publicly available through Github and public links to data servers.  
727 The Columbia tropical cyclone hazard model (CHAZ) is available on Github <https://github.com/c13225/CHAZ>. LitPop is available online at <https://www.research-collection.ethz.ch/handle/20.500.11850/331316>. EM-DAT is available online at <https://public.emdat.be/>.  
730

## 731 **References**

732 Aerts, J. C., N. Lin, W. Botzen, K. Emanuel, and H. de Moel, 2013: Low-probability flood risk  
733 modeling for New York City. *Risk Analysis*, **33** (5), 772–788, publisher: Wiley Online Library.

734 Bersales, L. G. S., 2017: 2015 Family Income and Expenditure Survey. Tech. rep., Philip-  
735 pine Statistics Authority. URL <https://psa.gov.ph/sites/default/files/FIES%202015%20Final%20Report.pdf>.  
736

737 Beven, J. L., and Coauthors, 2008: Atlantic Hurricane Season of 2005. *Monthly Weather Re-*  
738 *view*, **136** (3), 1109–1173, doi:10.1175/2007MWR2074.1, URL <https://journals.ametsoc.org/view/journals/mwre/136/3/2007mwr2074.1.xml>, publisher: American Meteorological Society  
739 Section: Monthly Weather Review.  
740

741 Bloemendaal, N., H. de Moel, S. Muis, I. D. Haigh, and J. C. J. H. Aerts, 2020a: Estima-  
742 tion of global tropical cyclone wind speed probabilities using the STORM dataset. *Scien-*  
743 *tific Data*, **7** (1), 377, doi:10.1038/s41597-020-00720-x, URL <https://www.nature.com/articles/s41597-020-00720-x>, number: 1 Publisher: Nature Publishing Group.  
744

745 Bloemendaal, N., I. D. Haigh, H. de Moel, S. Muis, R. J. Haarsma, and J. C. J. H. Aerts,  
746 2020b: Generation of a global synthetic tropical cyclone hazard dataset using STORM. *Sci-*  
747 *entific Data*, **7 (1)**, 40, doi:10.1038/s41597-020-0381-2, URL <https://www.nature.com/articles/s41597-020-0381-2>, number: 1 Publisher: Nature Publishing Group.

749 Board, J., 2019: In the path of the storm: Life in Batanes on the Philip-  
750 pines' typhoon track. *Channel News Asia*, URL <https://www.channelnewsasia.com/asia/islands-in-the-path-of-typhoons-life-in-batanes-philippines-792076>.

752 Chang, D., S. Amin, and K. Emanuel, 2020: Modeling and Parameter Estimation of Hurricane  
753 Wind Fields with Asymmetry. *Journal of Applied Meteorology and Climatology*, **59 (4)**, 687–  
754 705, doi:10.1175/JAMC-D-19-0126.1, URL <https://journals.ametsoc.org/view/journals/apme/59/4/jamc-d-19-0126.1.xml>, publisher: American Meteorological Society Section: Journal of  
755 Applied Meteorology and Climatology.

757 Chavas, D. R., and J. A. Knaff, 2022: A simple model for predicting the tropi-  
758 cal cyclone radius of maximum wind from outer size. *Weather and Forecasting*, -  
759 **1 (aop)**, doi:10.1175/WAF-D-21-0103.1, URL <https://journals.ametsoc.org/view/journals/wefo/aop/WAF-D-21-0103.1/WAF-D-21-0103.1.xml>, publisher: American Meteorological Society  
760 Section: Weather and Forecasting.

762 Chavas, D. R., N. Lin, and K. Emanuel, 2015: A Model for the Complete Radial Structure of  
763 the Tropical Cyclone Wind Field. Part I: Comparison with Observed Structure. *Journal of the*  
764 *Atmospheric Sciences*, **72 (9)**, 3647–3662, doi:10.1175/JAS-D-15-0014.1, URL <https://journals.ametsoc.org/doi/full/10.1175/JAS-D-15-0014.1>, publisher: American Meteorological Society.

766 Cinco, T. A., and Coauthors, 2016: Observed trends and impacts of tropical cy-  
767 clones in the Philippines. *International Journal of Climatology*, **36 (14)**, 4638–4650,

768 doi:10.1002/joc.4659, URL <https://onlinelibrary.wiley.com/doi/abs/10.1002/joc.4659>, \_eprint:  
769 <https://onlinelibrary.wiley.com/doi/pdf/10.1002/joc.4659>.

770 Corporal-Lodangco, I. L., and L. M. Leslie, 2017: Climatology of Philippine tropical cyclone  
771 activity: 1945–2011. *International Journal of Climatology*, **37 (9)**, 3525–3539, publisher:  
772 Wiley Online Library.

773 Corporal-Lodangco, I. L., L. M. Leslie, and P. J. Lamb, 2016: Impacts of ENSO on Philippine  
774 tropical cyclone activity. *Journal of Climate*, **29 (5)**, 1877–1897.

775 Cutter, S. L., B. J. Boruff, and W. L. Shirley, 2003: Social Vulnerability to Environmental  
776 Hazards\*. *Social Science Quarterly*, **84 (2)**, 242–261, doi:<https://doi.org/10.1111/1540-6237.8402002>,  
777 URL <https://onlinelibrary.wiley.com/doi/abs/10.1111/1540-6237.8402002>, \_eprint:  
778 <https://onlinelibrary.wiley.com/doi/pdf/10.1111/1540-6237.8402002>.

779 Dee, D. P., and Coauthors, 2011: The ERA-Interim reanalysis: Configuration and performance of  
780 the data assimilation system. *Quarterly Journal of the Royal Meteorological Society*, **137 (656)**,  
781 553–597, URL <http://onlinelibrary.wiley.com/doi/10.1002/qj.828/full>.

782 del Rosario, E. D., ??: Final Report re Effects of Typhoon "Yolanda" (Haiyan). Tech. rep.,  
783 National Disaster Risk Reduction and Management Council, Republic of the Philippines, Que-  
784 zon City, Philippines, 148 pp. URL [https://ndrrmc.gov.ph/attachments/article/1329/FINAL\\_](https://ndrrmc.gov.ph/attachments/article/1329/FINAL_REPORT_re_Effects_of_Typhoon_YOLANDA_(HAIYAN)_06-09NOV2013.pdf)  
785 [REPORT\\_re\\_Effects\\_of\\_Typhoon\\_YOLANDA\\_\(HAIYAN\)\\_06-09NOV2013.pdf](https://ndrrmc.gov.ph/attachments/article/1329/FINAL_REPORT_re_Effects_of_Typhoon_YOLANDA_(HAIYAN)_06-09NOV2013.pdf).

786 Deuchert, E., and C. Felfe, 2015: The tempest: Short-and long-term consequences of a natu-  
787 ral disaster for children s development. *European Economic Review*, **80**, 280–294, publisher:  
788 Elsevier.

789 Dominguez, C., A. Jaramillo, and P. Cuéllar, 2021: Are the socioeconomic impacts  
790 associated with tropical cyclones in Mexico exacerbated by local vulnerability and  
791 ENSO conditions? *International Journal of Climatology*, **41 (S1)**, E3307–E3324,  
792 doi:10.1002/joc.6927, URL <https://onlinelibrary.wiley.com/doi/abs/10.1002/joc.6927>, \_eprint:  
793 <https://onlinelibrary.wiley.com/doi/pdf/10.1002/joc.6927>.

794 Doxsey-Whitfield, E., K. MacManus, S. B. Adamo, L. Pistolesi, J. Squires, O. Borkovska, and  
795 S. R. Baptista, 2015: Taking advantage of the improved availability of census data: a first look  
796 at the gridded population of the world, version 4. *Papers in Applied Geography*, **1 (3)**, 226–234,  
797 publisher: Taylor & Francis.

798 Eadie, P., M. E. Atienza, and M. Tan-Mullins, 2020: Livelihood and vulnerability in the wake of  
799 Typhoon Yolanda: lessons of community and resilience. *Natural Hazards*, **103 (1)**.

800 Eberenz, S., S. Lüthi, and D. N. Bresch, 2020a: Regional tropical cyclone impact functions for  
801 globally consistent risk assessments. *Natural Hazards and Earth System Sciences Discussions*,  
802 1–29, doi:<https://doi.org/10.5194/nhess-2020-229>, URL [https://nhess.copernicus.org/preprints/  
803 nhess-2020-229/](https://nhess.copernicus.org/preprints/nhess-2020-229/), publisher: Copernicus GmbH.

804 Eberenz, S., D. Stocker, T. Rösli, and D. N. Bresch, 2020b: Asset exposure data for global  
805 physical risk assessment. *Earth System Science Data*, **12 (2)**, 817–833, publisher: Copernicus  
806 Publication.

807 Ehrhart, B., S. Mildenhall, A. Podlaha, and S. Bowen, 2014: Annual Global Climate and Catastro-  
808 phe Report: Impact Forecasting — 2013. Tech. rep., Aon Benfield. URL [http://thoughtleadership.  
809 aon.com/Documents/20140113\\_ab\\_if\\_annual\\_climate\\_catastrophe\\_report.pdf](http://thoughtleadership.aon.com/Documents/20140113_ab_if_annual_climate_catastrophe_report.pdf).

810 Elliott, R. J. R., E. Strobl, and P. Sun, 2015: The local impact of typhoons on economic activity  
811 in China: A view from outer space. *Journal of Urban Economics*, **88**, 50–66, doi:10.1016/j.jue.  
812 2015.05.001, URL <http://www.sciencedirect.com/science/article/pii/S0094119015000340>.

813 Emanuel, K., 2005: Increasing destructiveness of tropical cyclones over the past 30 years. *Nature*,  
814 **436 (7051)**, 686–688, doi:10.1038/nature03906, URL <https://www.nature.com/articles/nature03906>, number: 7051 Publisher: Nature Publishing Group.

816 Emanuel, K., 2011: Global warming effects on US hurricane damage. *Weather, Climate, and*  
817 *Society*, **3 (4)**, 261–268.

818 Ericta, C. N., and E. Fabian, 2009: A Documentation of the Philippines’ Family Income and  
819 Expenditure Survey. Working Paper 2009-18, PIDS Discussion Paper Series. URL <https://www.econstor.eu/handle/10419/126778>.

821 Feenstra, R. C., R. Inklaar, and M. P. Timmer, 2015: The next generation of the Penn World Table.  
822 *American economic review*, **105 (10)**, 3150–82.

823 Fiedler, T., A. J. Pitman, K. Mackenzie, N. Wood, C. Jakob, and S. E. Perkins-Kirkpatrick,  
824 2021: Business risk and the emergence of climate analytics. *Nature Climate Change*,  
825 **11 (2)**, 87–94, doi:10.1038/s41558-020-00984-6, URL <https://www.nature.com/articles/s41558-020-00984-6>, number: 2 Publisher: Nature Publishing Group.

827 Field, C. B., and Coauthors, 2012: *Managing the Risks of Extreme Events and Disasters to*  
828 *Advance Climate Change Adaptation. A Special Report of Working Groups I and II of IPCC*  
829 *Intergovernmental Panel on Climate Change*. Cambridge University Press, Cambridge, URL  
830 <https://boris.unibe.ch/71442/>.

831 Gori, A., N. Lin, D. Xi, and K. Emanuel, 2022: Tropical cyclone climatology change greatly  
832 exacerbates US extreme rainfall–surge hazard. *Nature Climate Change*, 1–8, doi:10.1038/  
833 s41558-021-01272-7, URL <https://www.nature.com/articles/s41558-021-01272-7>, publisher:  
834 Nature Publishing Group.

835 Guha-Sapir, D., R. Below, and P. Hoyois, 2003: EM-DAT: The CRED/OFDA International Disaster  
836 Database. Tech. rep., Université Catholique de Louvain, Brussels, Belgium. URL [www.emdat.be](http://www.emdat.be).

837 Hallegatte, S., A. Vogt-Schilb, M. Bangalore, and J. Rozenberg, 2016: *Unbreakable: building the*  
838 *resilience of the poor in the face of natural disasters*. World Bank Publications.

839 Holland, G. J., 1980: An analytic model of the wind and pressure profiles in hurricanes. *Monthly*  
840 *weather review*, **108 (8)**, 1212–1218.

841 Hsu, S. A., and Z. Yan, 1998: A note on the radius of maximum wind for hurricanes. *Journal of*  
842 *coastal research*, **14 (2)**.

843 Jing, R., and N. Lin, 2020: An Environment-Dependent Probabilistic Trop-  
844 ical Cyclone Model. *Journal of Advances in Modeling Earth Systems*,  
845 **12 (3)**, e2019MS001975, doi:<https://doi.org/10.1029/2019MS001975>, URL  
846 <https://agupubs.onlinelibrary.wiley.com/doi/abs/10.1029/2019MS001975>,  
\_eprint:  
847 <https://agupubs.onlinelibrary.wiley.com/doi/pdf/10.1029/2019MS001975>.

848 Klotz, B. W., and H. Jiang, 2017: Examination of surface wind asymmetries in tropical cyclones.  
849 Part I: General structure and wind shear impacts. *Monthly Weather Review*, **145 (10)**, 3989–4009,  
850 publisher: American Meteorological Society.

851 Knaff, J. A., S. P. Longmore, R. T. DeMaria, and D. A. Molenaar, 2015: Improved  
852 Tropical-Cyclone Flight-Level Wind Estimates Using Routine Infrared Satellite Recon-

853 naissance. *Journal of Applied Meteorology and Climatology*, **54** (2), 463–478, doi:  
854 10.1175/JAMC-D-14-0112.1, URL [https://journals.ametsoc.org/jamc/article/54/2/463/13954/  
855 Improved-Tropical-Cyclone-Flight-Level-Wind](https://journals.ametsoc.org/jamc/article/54/2/463/13954/Improved-Tropical-Cyclone-Flight-Level-Wind), publisher: American Meteorological Society.

856 Knapp, K. R., M. C. Kruk, D. H. Levinson, H. J. Diamond, and C. J. Neumann, 2010: The  
857 international best track archive for climate stewardship (IBTrACS) unifying tropical cyclone  
858 data. *Bulletin of the American Meteorological Society*, **91** (3), 363–376, publisher: American  
859 Meteorological Society.

860 Knutson, T., and Coauthors, 2020: Tropical cyclones and climate change assessment: Part II:  
861 Projected response to anthropogenic warming. *Bulletin of the American Meteorological Society*,  
862 **101** (3), E303–E322, publisher: American Meteorological Society.

863 Lagmay, A. M. F., and Coauthors, 2015: Devastating storm surges of Typhoon Haiyan. *Inter-  
864 national Journal of Disaster Risk Reduction*, **11**, 1–12, doi:10.1016/j.ijdr.2014.10.006, URL  
865 <https://www.sciencedirect.com/science/article/pii/S2212420914000922>.

866 Lee, C.-Y., S. J. Camargo, A. H. Sobel, and M. K. Tippett, 2020: Statistical–dynamical downscaling  
867 projections of tropical cyclone activity in a warming climate: Two diverging genesis scenarios.  
868 *Journal of Climate*, **33** (11), 4815–4834.

869 Lee, C.-Y., M. K. Tippett, A. H. Sobel, and S. J. Camargo, 2016: Autoregressive Model-  
870 ing for Tropical Cyclone Intensity Climatology. *Journal of Climate*, **29** (21), 7815–7830,  
871 doi:10.1175/JCLI-D-15-0909.1, URL [https://journals.ametsoc.org/view/journals/clim/29/21/  
872 jcli-d-15-0909.1.xml](https://journals.ametsoc.org/view/journals/clim/29/21/jcli-d-15-0909.1.xml), publisher: American Meteorological Society Section: Journal of Cli-  
873 mate.

- 874 Lee, C.-Y., M. K. Tippett, A. H. Sobel, and S. J. Camargo, 2018: An Environ-  
875 mentally Forced Tropical Cyclone Hazard Model. *Journal of Advances in Mod-*  
876 *eling Earth Systems*, **10** (1), 223–241, doi:<https://doi.org/10.1002/2017MS001186>,  
877 URL <https://agupubs.onlinelibrary.wiley.com/doi/abs/10.1002/2017MS001186>, \_eprint:  
878 <https://agupubs.onlinelibrary.wiley.com/doi/pdf/10.1002/2017MS001186>.
- 879 Leonard, M., and Coauthors, 2014: A compound event framework for understanding extreme  
880 impacts. *Wiley Interdisciplinary Reviews: Climate Change*, **5** (1), 113–128, doi:10.1002/wcc.  
881 252, URL <http://onlinelibrary.wiley.com/doi/10.1002/wcc.252/abstract>.
- 882 Lin, I.-I., I.-F. Pun, and C.-C. Lien, 2014: “Category-6” supertyphoon Haiyan in global warming  
883 hiatus: Contribution from subsurface ocean warming. *Geophysical Research Letters*, **41** (23),  
884 8547–8553, publisher: Wiley Online Library.
- 885 Lin, N., and D. Chavas, 2012: On hurricane parametric wind and applications in storm surge mod-  
886 eling. *Journal of Geophysical Research: Atmospheres*, **117** (D9), doi:[https://doi.org/10.1029/](https://doi.org/10.1029/2011JD017126)  
887 [2011JD017126](https://doi.org/10.1029/2011JD017126), URL <https://agupubs.onlinelibrary.wiley.com/doi/abs/10.1029/2011JD017126>,  
888 \_eprint: <https://agupubs.onlinelibrary.wiley.com/doi/pdf/10.1029/2011JD017126>.
- 889 Lin, N., K. Emanuel, M. Oppenheimer, and E. Vanmarcke, 2012: Physically based assessment of  
890 hurricane surge threat under climate change. *Nature Climate Change*, **2** (6), 462–467, doi:10.  
891 1038/nclimate1389, URL <https://www.nature.com/articles/nclimate1389>, number: 6 Publisher:  
892 Nature Publishing Group.
- 893 Lin, N., K. A. Emanuel, J. A. Smith, and E. Vanmarcke, 2010: Risk assessment of hurricane storm  
894 surge for New York City. *Journal of Geophysical Research: Atmospheres*, **115** (D18), publisher:  
895 Wiley Online Library.

- 896 Lyon, B., and S. J. Camargo, 2009: The seasonally-varying influence of ENSO on rainfall and  
897 tropical cyclone activity in the Philippines. *Climate Dynamics*, **32** (1), 125–141, doi:10.1007/  
898 s00382-008-0380-z, URL <https://doi.org/10.1007/s00382-008-0380-z>.
- 899 Mas, E., J. Bricker, S. Kure, B. Adriano, C. Yi, A. Suppasri, and S. Koshimura, 2015: Field survey  
900 report and satellite image interpretation of the 2013 Super Typhoon Haiyan in the Philippines.  
901 *Natural Hazards and Earth System Sciences*, **15** (4), 805–816, publisher: Copernicus GmbH.
- 902 Matthews, T., R. L. Wilby, and C. Murphy, 2019: An emerging tropical cyclone–deadly heat  
903 compound hazard. *Nature Climate Change*, **9** (8), 602–606, doi:10.1038/s41558-019-0525-6,  
904 URL <https://www.nature.com/articles/s41558-019-0525-6>.
- 905 Meiler, S., T. Vogt, N. Bloemendaal, A. Ciullo, C.-Y. Lee, S. Camargo, K. Emanuel, and D. Bresch,  
906 2022: Intercomparison of regional loss estimates from global synthetic tropical cyclone mod-  
907 els. Tech. rep. doi:10.21203/rs.3.rs-1429968/v1, URL [https://www.researchsquare.com/article/  
908 rs-1429968/v1](https://www.researchsquare.com/article/rs-1429968/v1), iSSN: 2693-5015 Type: article.
- 909 Noy, I., 2009: The macroeconomic consequences of disasters. *Journal of Development economics*,  
910 **88** (2), 221–231, publisher: Elsevier.
- 911 OCHA, 2022: Philippines: Super Typhoon Rai (Odette). Tech.  
912 Rep. 7, United Nations. URL [https://reliefweb.int/report/philippines/  
913 philippines-super-typhoon-rai-odette-situation-report-no-7-25-march-2022](https://reliefweb.int/report/philippines/philippines-super-typhoon-rai-odette-situation-report-no-7-25-march-2022).
- 914 Ribera, P., R. García Herrera, and L. Gimeno, 2008: Historical deadly typhoons in the Philippines.  
915 *Weather*, **63** (7), 194, publisher: John Wiley & Sons LTD.
- 916 Rodrigo, S. M. T., C. L. Villanoy, J. C. Briones, P. H. T. Bilgera, O. C. Cabrera, and G. T. T. Narisma,  
917 2018: The mapping of storm surge-prone areas and characterizing surge-producing cyclones in

918 Leyte Gulf, Philippines. *Natural Hazards*, **92** (3), 1305–1320, doi:10.1007/s11069-018-3252-9,  
919 URL <https://doi.org/10.1007/s11069-018-3252-9>.

920 Román, M. O., and Coauthors, 2018: NASA’s Black Marble nighttime lights product suite. *Remote*  
921 *Sensing of Environment*, **210**, 113–143, publisher: Elsevier.

922 Rowe, D., 2021: Personal communication.

923 Sakai, Y., J. P. Estudillo, N. Fuwa, Y. Higuchi, and Y. Sawada, 2017: Do natural disasters affect the  
924 poor disproportionately? Price change and welfare impact in the aftermath of Typhoon Milenyo  
925 in the rural Philippines. *World Development*, **94**, 16–26, publisher: Elsevier.

926 Sato, T., and T. Nakasu, 2011: 2009 Typhoon Ondoy Flood Disasters in Metro Manila. *Natural*  
927 *Disaster Research Report*, **45**, 63–74.

928 Sobel, A. H., C.-Y. Lee, S. J. Camargo, K. T. Mandli, K. A. Emanuel, P. Mukhopadhyay, and  
929 M. Mahakur, 2019: Tropical cyclone hazard to Mumbai in the recent historical climate. *Monthly*  
930 *Weather Review*, **147** (7), 2355–2366.

931 Soria, J. L. A., and Coauthors, 2016: Repeat storm surge disasters of Typhoon Haiyan and its 1897  
932 predecessor in the Philippines. *Bulletin of the American Meteorological Society*, **97** (1), 31–48,  
933 publisher: American Meteorological Society.

934 Strobl, E., 2011: The Economic Growth Impact of Hurricanes: Evidence from U.S. Coastal  
935 Counties. *The Review of Economics and Statistics*, **93** (2), 575–589, URL [https://econpapers.](https://econpapers.repec.org/article/tprrestat/v_3a93_3ay_3a2011_3ai_3a2_3ap_3a575-589.htm)  
936 [repec.org/article/tprrestat/v\\_3a93\\_3ay\\_3a2011\\_3ai\\_3a2\\_3ap\\_3a575-589.htm](https://econpapers.repec.org/article/tprrestat/v_3a93_3ay_3a2011_3ai_3a2_3ap_3a575-589.htm), publisher: MIT  
937 Press.

938 Tellman, B., C. Schank, B. Schwarz, P. D. Howe, and A. de Sherbinin, 2020: Using Disaster  
939 Outcomes to Validate Components of Social Vulnerability to Floods: Flood Deaths and Prop-

erty Damage across the USA. *Sustainability*, **12** (15), 6006, doi:10.3390/su12156006, URL  
https://www.mdpi.com/2071-1050/12/15/6006, number: 15 Publisher: Multidisciplinary Digital  
Publishing Institute.

Uhlhorn, E. W., B. W. Klotz, T. Vukicevic, P. D. Reasor, and R. F. Rogers, 2014: Observed Hurricane Wind Speed Asymmetries and Relationships to Motion and Environmental Shear. *Monthly Weather Review*, **142** (3), 1290–1311, doi:10.1175/MWR-D-13-00249.1, URL https://journals.ametsoc.org/mwr/article/142/3/1290/71766/Observed-Hurricane-Wind-Speed-Asymmetries-and, publisher: American Meteorological Society.

Vecchi, G. A., and Coauthors, 2019: Tropical cyclone sensitivities to CO2 doubling: roles of atmospheric resolution, synoptic variability and background climate changes. *Climate Dynamics*, **53** (9), 5999–6033, doi:10.1007/s00382-019-04913-y, URL https://www.dropbox.com/s/zu5uxctekjtmwj8/vecchi-tropical-2019.pdf?dl=0.

Vickery, P. J., J. Lin, P. F. Skerlj, L. A. Twisdale Jr, and K. Huang, 2006a: HAZUS-MH hurricane model methodology. I: Hurricane hazard, terrain, and wind load modeling. *Natural Hazards Review*, **7** (2), 82–93, publisher: American Society of Civil Engineers.

Vickery, P. J., P. F. Skerlj, J. Lin, L. A. Twisdale Jr, M. A. Young, and F. M. Lavelle, 2006b: HAZUS-MH hurricane model methodology. II: Damage and loss estimation. *Natural Hazards Review*, **7** (2), 94–103, publisher: American Society of Civil Engineers.

Walsh, B., and S. Hallegatte, 2020: Measuring Natural Risks in the Philippines: Socioeconomic Resilience and Wellbeing Losses. *Economics of Disasters and Climate Change*, **4** (2), 249–293, doi:10.1007/s41885-019-00047-x, URL https://doi.org/10.1007/s41885-019-00047-x.

- 962 Walsh, B. J., and S. Hallegatte, 2019: *Measuring Natural Risks in the Philippines: Socioeconomic*  
963 *Resilience and Wellbeing Losses*. The World Bank.
- 964 Watson, C. C., and M. E. Johnson, 2004: Hurricane Loss Estimation Models: Opportunities for  
965 Improving the State of the Art. *Bulletin of the American Meteorological Society*, **85 (11)**, 1713–  
966 1726, doi:10.1175/BAMS-85-11-1713, URL [https://journals.ametsoc.org/view/journals/bams/](https://journals.ametsoc.org/view/journals/bams/85/11/bams-85-11-1713.xml)  
967 [85/11/bams-85-11-1713.xml](https://journals.ametsoc.org/view/journals/bams/85/11/bams-85-11-1713.xml), publisher: American Meteorological Society Section: Bulletin of  
968 the American Meteorological Society.
- 969 Willoughby, H. E., R. W. R. Darling, and M. E. Rahn, 2006: Parametric representation of the  
970 primary hurricane vortex. Part II: A new family of sectionally continuous profiles. *Monthly*  
971 *weather review*, **134 (4)**, 1102–1120.
- 972 Wilson, K., and J. W. Baldwin, 2021: Estimating Tropical Cyclone Vulnerability: A Review of  
973 Different Open-Source Approaches. *Hurricane Risk in a Changing Climate*, Springer, in Review.
- 974 World Bank, 2021: Wealth Accounting. URL [https://datacatalog.worldbank.org/search/dataset/](https://datacatalog.worldbank.org/search/dataset/0042066)  
975 [0042066](https://datacatalog.worldbank.org/search/dataset/0042066).
- 976 Xi, D., N. Lin, and J. Smith, 2020: Evaluation of a Physics-Based Tropical Cyclone Rainfall  
977 Model for Risk Assessment. *Journal of Hydrometeorology*, **21 (9)**, 2197–2218, doi:10.1175/  
978 JHM-D-20-0035.1, URL [https://journals.ametsoc.org/view/journals/hydr/21/9/jhmD200035.](https://journals.ametsoc.org/view/journals/hydr/21/9/jhmD200035.xml)  
979 [xml](https://journals.ametsoc.org/view/journals/hydr/21/9/jhmD200035.xml), publisher: American Meteorological Society Section: Journal of Hydrometeorology.
- 980 Yamin, L. E., A. I. Hurtado, A. H. Barbat, and O. D. Cardona, 2014: Seismic and wind vulnerability  
981 assessment for the GAR-13 global risk assessment. *International Journal of Disaster Risk*  
982 *Reduction*, **10**, 452–460, doi:10.1016/j.ijdr.2014.05.007, URL [http://www.sciencedirect.com/](http://www.sciencedirect.com/science/article/pii/S2212420914000466)  
983 [science/article/pii/S2212420914000466](http://www.sciencedirect.com/science/article/pii/S2212420914000466).

984 Yang, Q., C.-Y. Lee, M. K. Tippett, D. R. Chavas, and T. R. Knutson, 2022:  
985 Machine learning based hurricane wind reconstruction. *Weather and Forecasting*, -  
986 **1 (aop)**, doi:10.1175/WAF-D-21-0077.1, URL [https://journals.ametsoc.org/view/journals/wefo/  
987 aop/WAF-D-21-0077.1/WAF-D-21-0077.1.xml](https://journals.ametsoc.org/view/journals/wefo/aop/WAF-D-21-0077.1/WAF-D-21-0077.1.xml), publisher: American Meteorological Society  
988 Section: Weather and Forecasting.

989 Yonson, R., I. Noy, and J. Gaillard, 2018: The measurement of disaster risk: An example from  
990 tropical cyclones in the Philippines. *Review of Development Economics*, **22 (2)**, 736–765, doi:  
991 10.1111/rode.12365, URL <https://onlinelibrary.wiley.com/doi/abs/10.1111/rode.12365>, \_eprint:  
992 <https://onlinelibrary.wiley.com/doi/pdf/10.1111/rode.12365>.

993 Zscheischler, J., and Coauthors, 2018: Future climate risk from compound events. *Nature Climate  
994 Change*, 1.

995 **LIST OF FIGURES**

996 **Fig. 1. Contrasting tropical cyclone density and socioeconomic resilience in the northern versus**  
 997 **southern Philippines.** (Left) Number of tropical storms and typhoons per year making  
 998 landfall in different regions of the Philippines; (middle) map and names of regions in the  
 999 Philippines (adapted from philippines.kosgep.org); (right) average socioeconomic resilience  
 1000 in different regions of the Philippines. Socioeconomic resilience is defined here as the ratio  
 1001 of expected asset losses to wellbeing losses in Walsh and Hallegatte (2020), from which the  
 1002 right panel of this figure is also adapted. Wellbeing losses are calculated using household  
 1003 survey data about consumption habits across the Philippines. . . . . 48

1004 **Fig. 2. Schematic of our TC risk modeling workflow.** Layers for hazard, vulnerability, and  
 1005 exposed value are combined to model asset losses from tropical cyclones. Details of each  
 1006 layer are described in Section 2. . . . . 49

1007 **Fig. 3. Example of observed versus synthetic landfalling TCs.** Sample of 200 landfalling TC  
 1008 tracks from (a) IBTrACS and (b) CHAZ. First landfall in the Philippines is demarcated with  
 1009 a star, and tracks are shaded by intensity at first landfall. . . . . 50

1010 **Fig. 4. Wind swath calculation schematic and resulting swaths for highly destructive historical**  
 1011 **TCs.** Moving from left to right: 1) information on maximum sustained wind speed, latitude,  
 1012 and radius of maximum wind along TC tracks is used to determine 2) profiles of wind with  
 1013 radius from the center of the storm, which is 3) placed on a latitude-longitude grid and  
 1014 combined with a correction for asymmetry to determine wind fields at each point in time,  
 1015 then 4) the wind swath is determined as the maximum across time of the wind fields when  
 1016 the storm is near land. Swaths corresponding to nine of the most costly historical storms  
 1017 affecting the Philippines are shown on the right hand side of the figure. . . . . 51

1018 **Fig. 5. Asset value across the Philippines according to LitPop.** Shaded is the estimated value of  
 1019 assets in 2014 USD for each 30 arcsec gridcell of LitPop. Major cities with high concentraion  
 1020 of assets are labeled. . . . . 52

1021 **Fig. 6. Example vulnerability curve based on Emanuel (2011).** Indicated are the two parameters  
 1022 that constrain the vulnerability curve:  $V_{thresh}$  (the minimum wind speed to have any damages)  
 1023 and  $V_{half}$  (the wind speed at which 50% of property value is lost). . . . . 53

1024 **Fig. 7. Historical TC-related damages for the Philippines over time from EM-DAT.** (a) has  
 1025 a linear y-axis and (b) has a log-scale y-axis, highlighting the many orders of magnitude  
 1026 damages from these events span. . . . . 54

1027 **Fig. 8. Sensitivity test of model ability to simulate historical damages considering different**  
 1028 **vulnerability parameter values ( $V_{half}$  and  $V_{thresh}$ ) in the Emanuel (2011) vulnerability**  
 1029 **curve.** The metrics evaluated are (a) Pearson’s  $r$ , (b) Kendall’s  $\tau$ , (c) Spearman’s  $r$ , (d)  
 1030 TDR (the natural logarithm of this quantity is shown), and (e) RMSF. For all panels, whiter  
 1031 shading indicates better correlation. Black X’s demarcate the optimal parameter values for  
 1032 each metric across all  $V_{half}$  and  $V_{thresh}$  values, and blue crosses demarcate the optimal  
 1033  $V_{half}$  parameter value when  $V_{thresh}$  is set to 25 m/s. Panels with multiple black X’s indicate  
 1034 optimal parameter sets with equivalent correlation. . . . . 55

1035 **Fig. 9. Simulated versus observed asset losses with a single national vulnerability curve fit to**  
 1036 **minimize RMSF.** Observed total damages are plotted against modeled total damages with  
 1037 (a) linear axes and (b) log-scale axes (b); black lines are one-to-one lines and events that  
 1038 result in losses in Manila are encircled in blue. (c) Bar chart of number of TC events with

1039 damage ratios less than 0.1, between 0.1 and 10, and greater than 10, split into events that  
1040 do not affect Manila (orange) versus those that do affect Manila (blue). As a reminder,  
1041 event damage ratio is equal to simulated damages for a TC divided by normalized reported  
1042 damages for the same TC. . . . . 56

1043 **Fig. 10. Prevalence of different roof materials for regions in the Philippines.** Bar charts for each  
1044 region showing percent of population occupying dwellings made of different roof materials,  
1045 according to the Philippines household survey data (FIES). The key in grey shows what roof  
1046 materials each x-axis number represents. . . . . 57

1047 **Fig. 11. Proportion of strong to weak roofs for regions in the Philippines.** Bar chart showing  
1048 number of strong divided by number of light roofs for each region in the Philippines. . . . . 58

1049 **Fig. 12. Correspondence of regional  $V_{half}$  to roof strength proportion, and resulting vulnera-**  
1050 **bility map from regression.** (a) Proportion of strong to weak roofs plotted against RMSF  
1051 fitted regional  $V_{half}$  values (blue circles) and linear fit between the two quantities (red line);  
1052 (b) regional  $V_{half}$  determined from proportion of strong to weak roofs in each province and  
1053 linear fit in panel a. Note that in panel a, NCR is the top-right point in the plot with the  
1054 highest  $V_{half}$  and strong roof proportion. . . . . 59

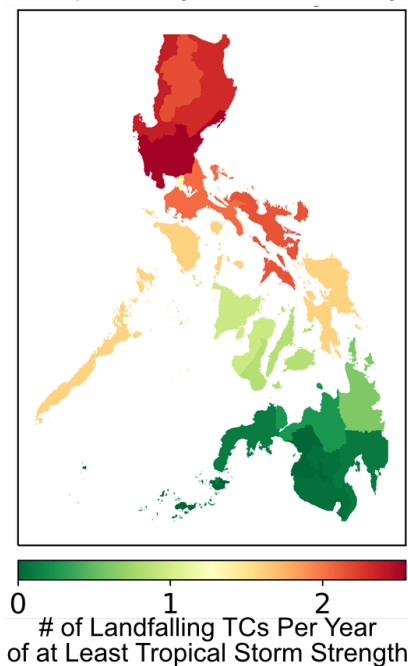
1055 **Fig. 13. Observed versus modeled damages for regionally varying vulnerability.** (a) Observed  
1056 total damages from EM-DAT plotted against modeled total damages calculated with the  
1057 regional varying vulnerability map; black line is the one-to-one line. (b) Same as panel a  
1058 but with reduced x and y-axis limits to highlight the prevalence of storms with zero modeled  
1059 damages. . . . . 60

1060 **Fig. 14. Damage simulation skill for national versus regionally varying vulnerability.** TDR across  
1061 regions for single national vulnerability curve (left) and regionally varying vulnerability  
1062 curves (right) and quantified as raw TDR (top) versus natural log of TDR (bottom). . . . . 61

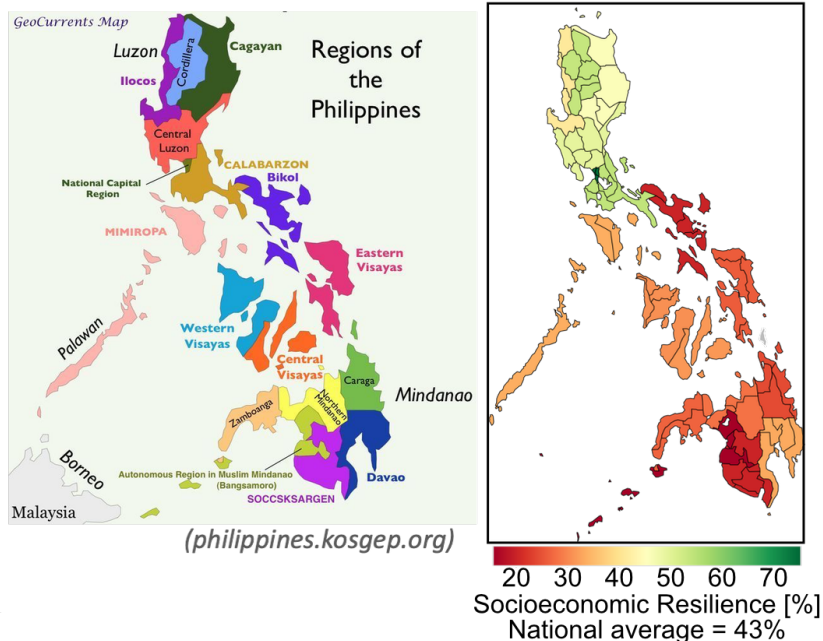
1063 **Fig. 15. Wind swath and asset losses for two notable Philippines-landfalling typhoons.** Wind  
1064 swath (contoured in purple— darker contours corresponds to faster wind speeds) and damages  
1065 (shaded red) for (left) typhoon Haiyan (Yolanda) and (right) Ketsana (Ondoy). The plot region  
1066 is constrained to the area of most direct impact by each storm, and at the top of each plot the  
1067 actual cost from EM-DAT is listed above the simulated damages summed across the entire  
1068 Philippines. . . . . 62

1069 **Fig. 16. Return periods for wind speed and asset losses for two regions in the Philippines.** Return  
1070 periods of different (top) maximum sustained wind speeds and (bottom) asset losses, for two  
1071 regions: (left) Manila/NCR and (right) Eastern Visayas. Simulated damages from IBTrACS  
1072 tracks are shown in black, while simulated damages from CHAZ tracks are shown in red; the  
1073 thin red lines designate return periods derived from each CHAZ intensity ensemble while the  
1074 thick dashed red line shows return periods from all the CHAZ tracks and intensity ensembles  
1075 together. . . . . 63

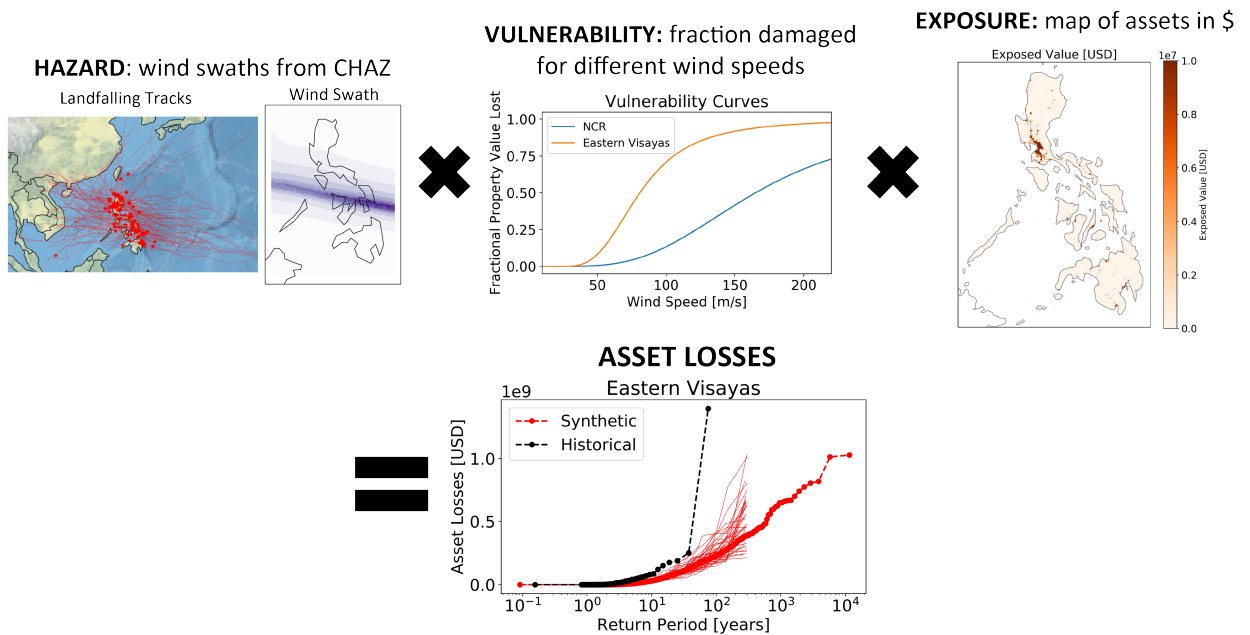
## Tropical Cyclone Density



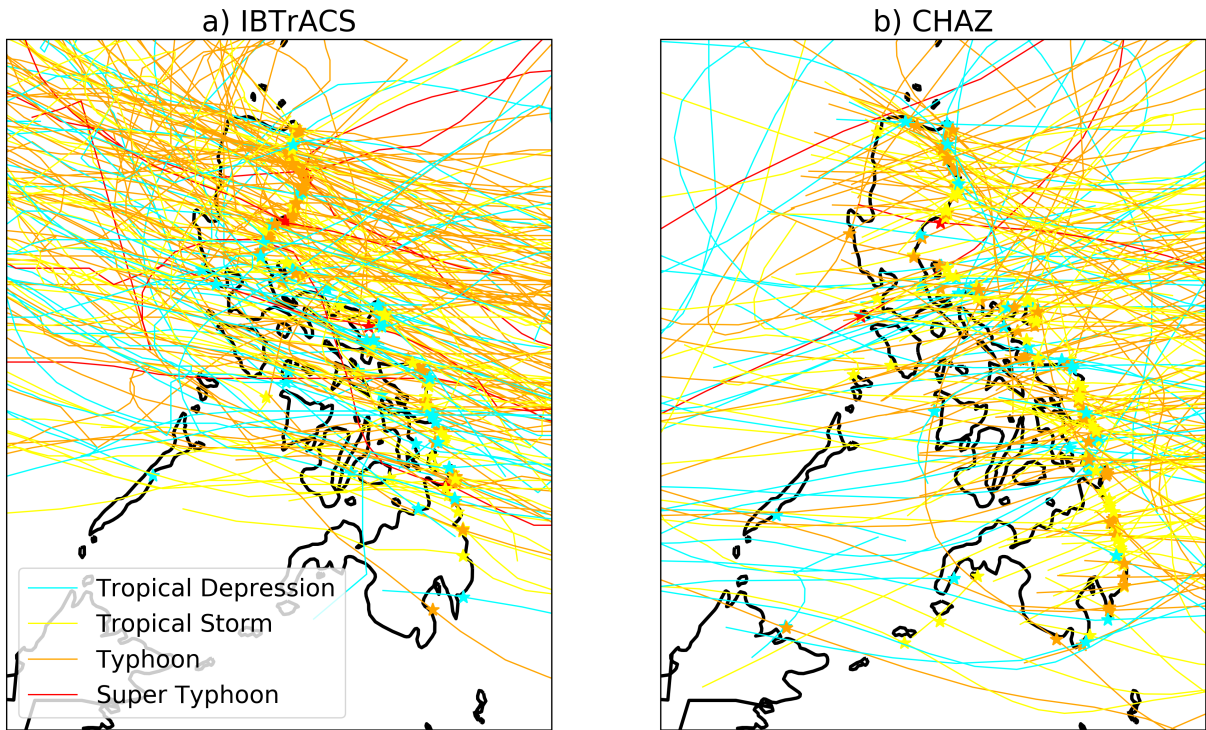
## Socioeconomic Resilience



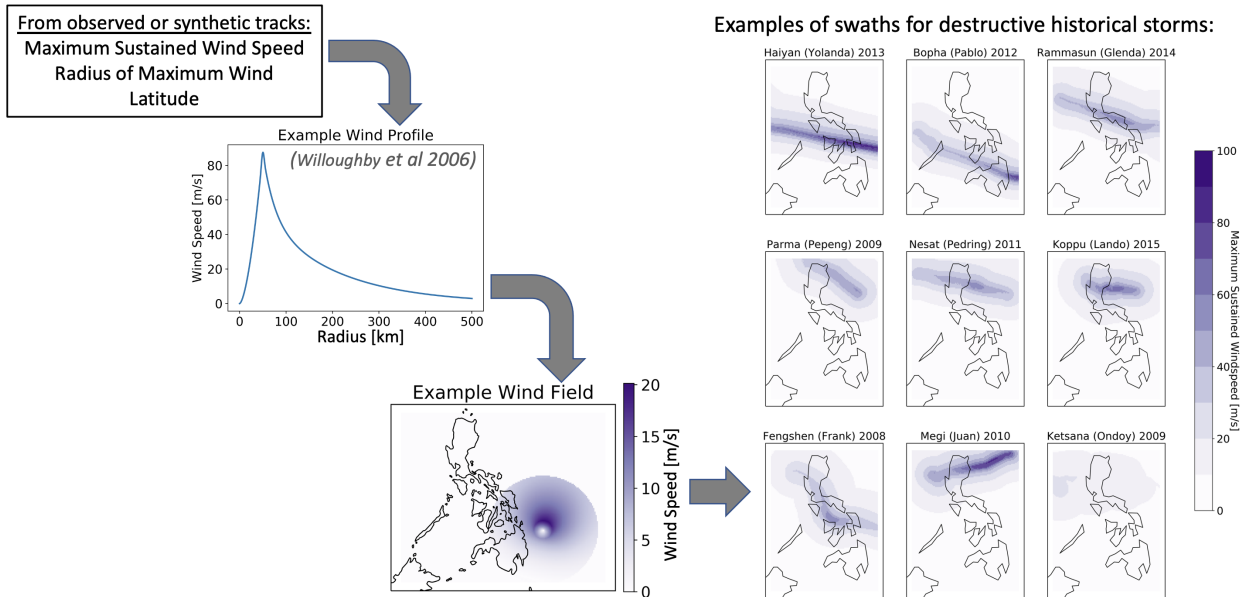
1076 FIG. 1. **Contrasting tropical cyclone density and socioeconomic resilience in the northern versus southern**  
 1077 **Philippines.** (Left) Number of tropical storms and typhoons per year making landfall in different regions of the  
 1078 Philippines; (middle) map and names of regions in the Philippines (adapted from philippines.kosgep.org); (right)  
 1079 average socioeconomic resilience in different regions of the Philippines. Socioeconomic resilience is defined  
 1080 here as the ratio of expected asset losses to wellbeing losses in Walsh and Hallegatte (2020), from which the  
 1081 right panel of this figure is also adapted. Wellbeing losses are calculated using household survey data about  
 1082 consumption habits across the Philippines.



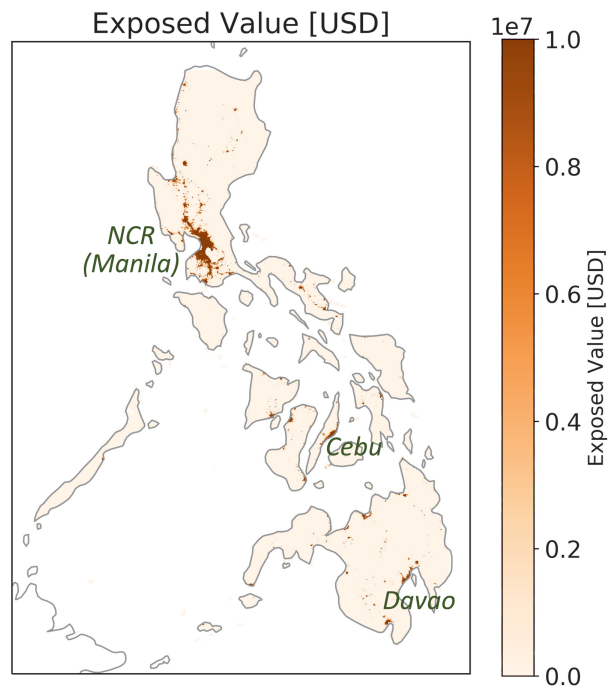
1083 FIG. 2. **Schematic of our TC risk modeling workflow.** Layers for hazard, vulnerability, and exposed value  
 1084 are combined to model asset losses from tropical cyclones. Details of each layer are described in Section 2.



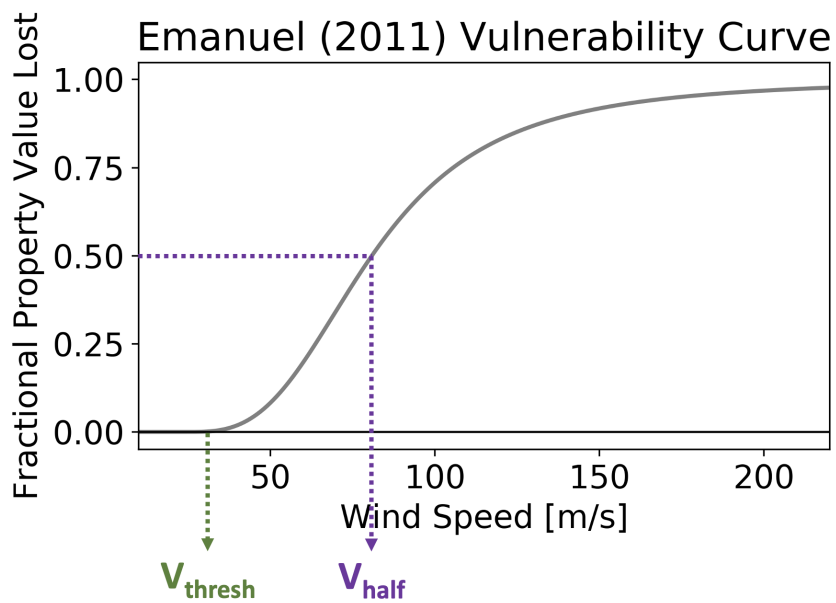
1085 **FIG. 3. Example of observed versus synthetic landfalling TCs.** Sample of 200 landfalling TC tracks from  
 1086 (a) IBTrACS and (b) CHAZ. First landfall in the Philippines is demarcated with a star, and tracks are shaded by  
 1087 intensity at first landfall.



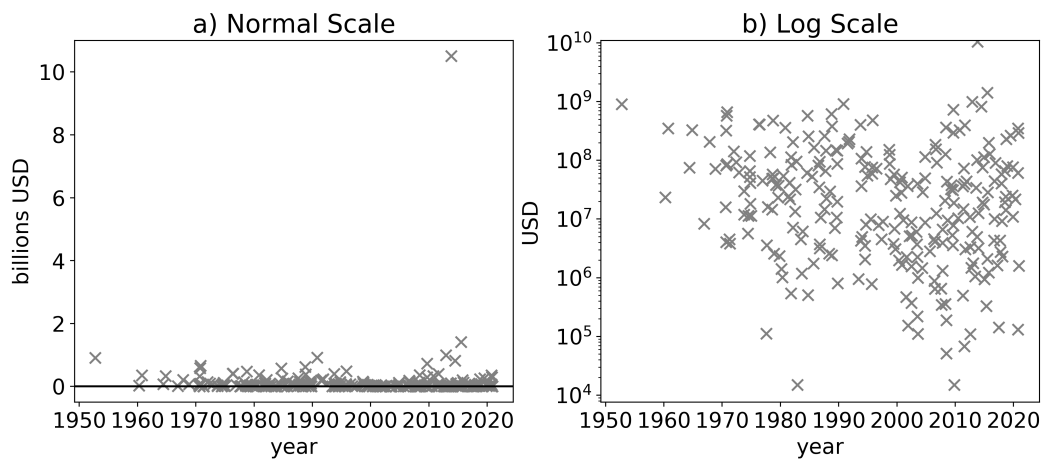
1088 **FIG. 4. Wind swath calculation schematic and resulting swaths for highly destructive historical TCs.**  
 1089 Moving from left to right: 1) information on maximum sustained wind speed, latitude, and radius of maximum  
 1090 wind along TC tracks is used to determine 2) profiles of wind with radius from the center of the storm, which is  
 1091 3) placed on a latitude-longitude grid and combined with a correction for asymmetry to determine wind fields at  
 1092 each point in time, then 4) the wind swath is determined as the maximum across time of the wind fields when the  
 1093 storm is near land. Swaths corresponding to nine of the most costly historical storms affecting the Philippines  
 1094 are shown on the right hand side of the figure.



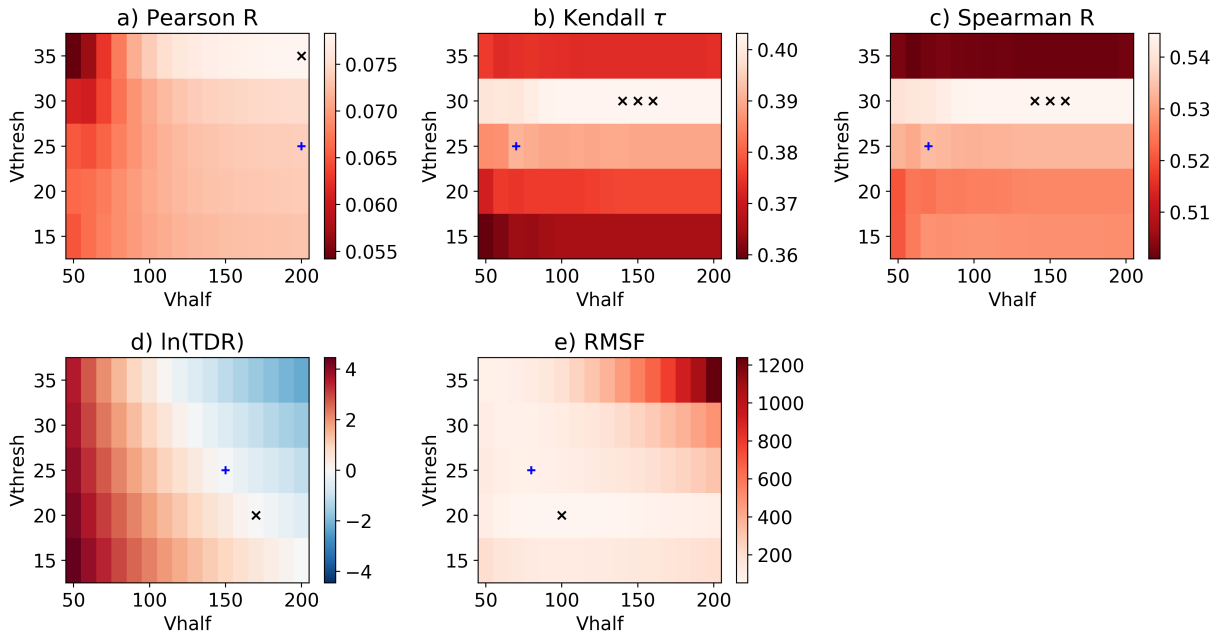
1095 FIG. 5. **Asset value across the Philippines according to LitPop.** Shaded is the estimated value of assets in  
 1096 2014 USD for each 30 arcsec gridcell of LitPop. Major cities with high concentraion of assets are labeled.



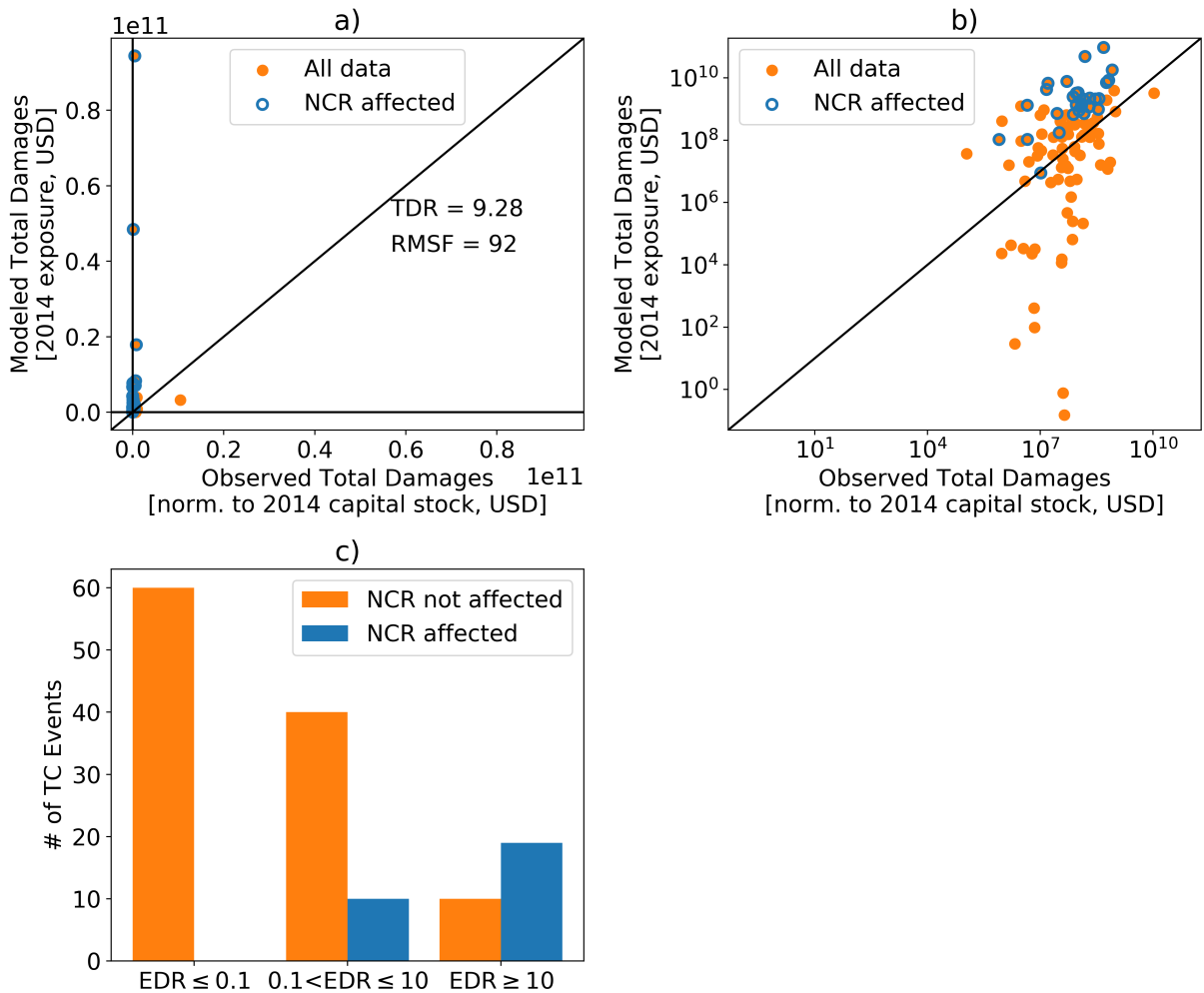
1097 FIG. 6. **Example vulnerability curve based on Emanuel (2011).** Indicated are the two parameters that  
 1098 constrain the vulnerability curve:  $V_{thresh}$  (the minimum wind speed to have any damages) and  $V_{half}$  (the wind  
 1099 speed at which 50% of property value is lost).



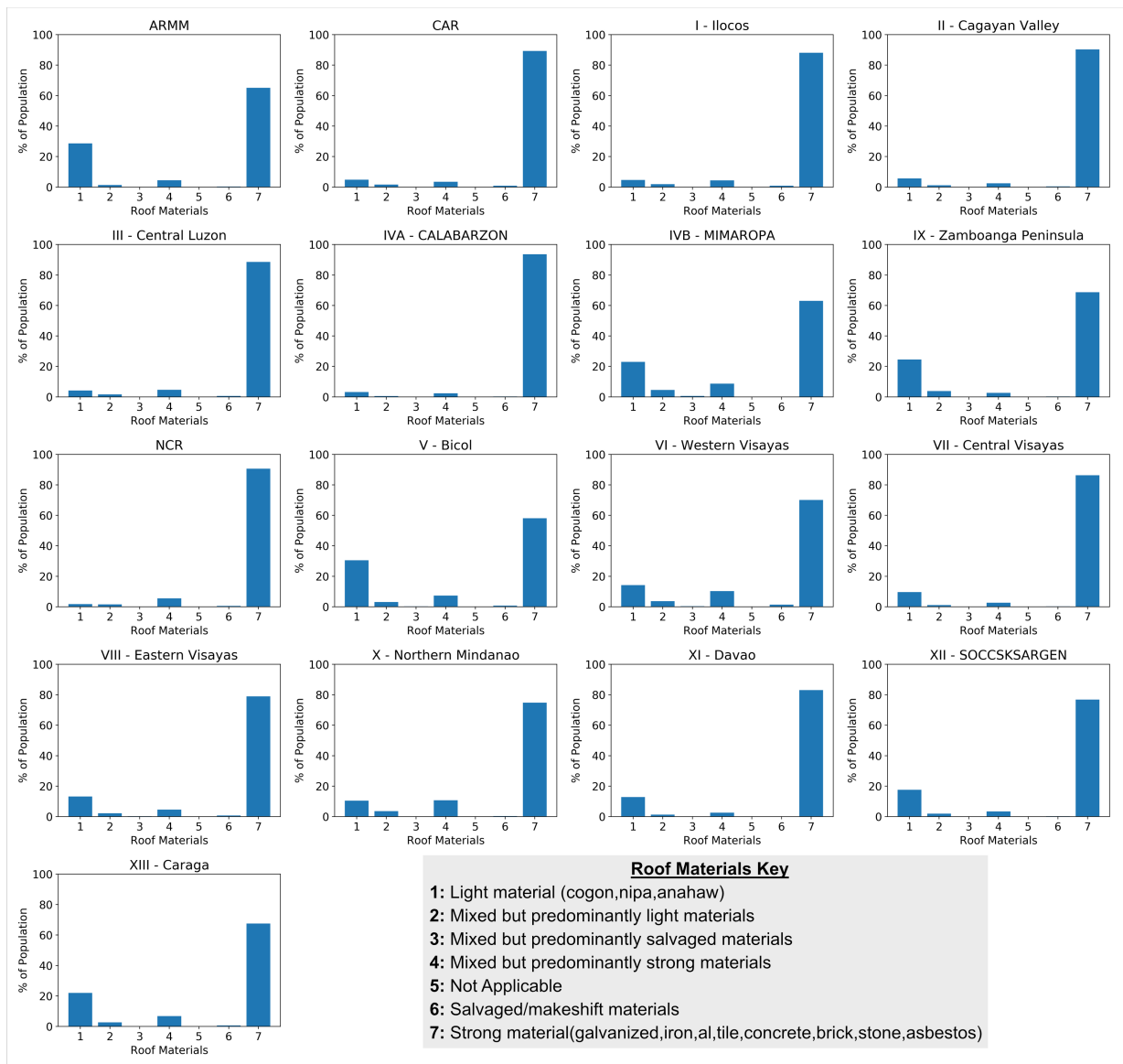
1100 FIG. 7. **Historical TC-related damages for the Philippines over time from EM-DAT.** (a) has a linear y-axis  
 1101 and (b) has a log-scale y-axis, highlighting the many orders of magnitude damages from these events span.



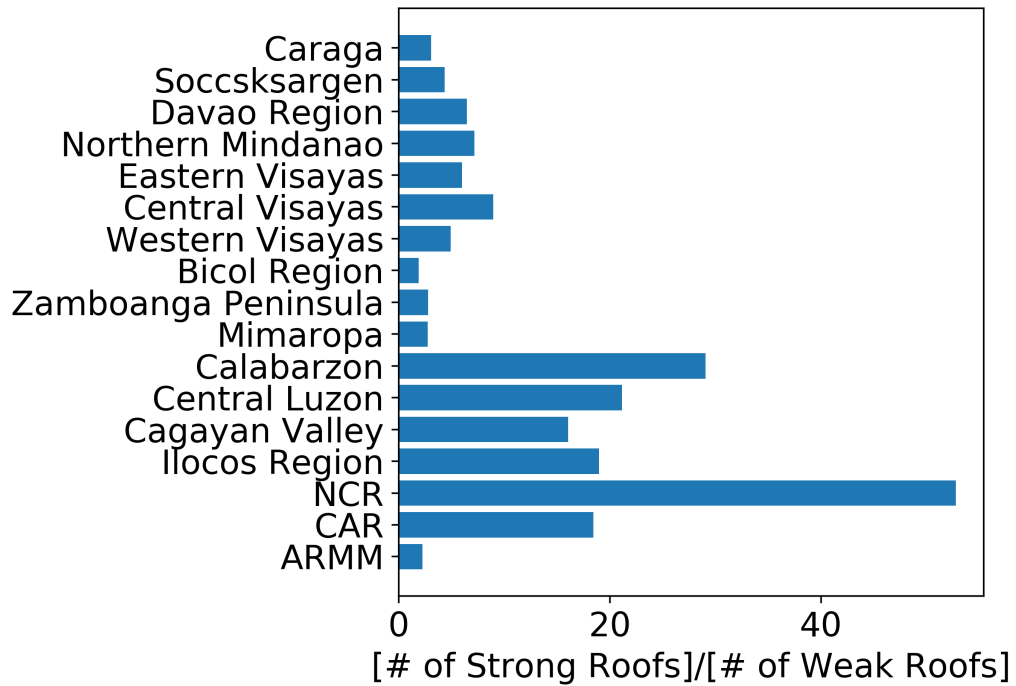
1102 **FIG. 8. Sensitivity test of model ability to simulate historical damages considering different vulnerability**  
 1103 **parameter values ( $V_{half}$  and  $V_{thresh}$ ) in the Emanuel (2011) vulnerability curve.** The metrics evaluated are  
 1104 (a) Pearson's  $r$ , (b) Kendall's  $\tau$ , (c) Spearman's  $r$ , (d) TDR (the natural logarithm of this quantity is shown),  
 1105 and (e) RMSF. For all panels, whiter shading indicates better correlation. Black X's demarcate the optimal  
 1106 parameter values for each metric across all  $V_{half}$  and  $V_{thresh}$  values, and blue crosses demarcate the optimal  
 1107  $V_{half}$  parameter value when  $V_{thresh}$  is set to 25 m/s. Panels with multiple black X's indicate optimal parameter  
 1108 sets with equivalent correlation.



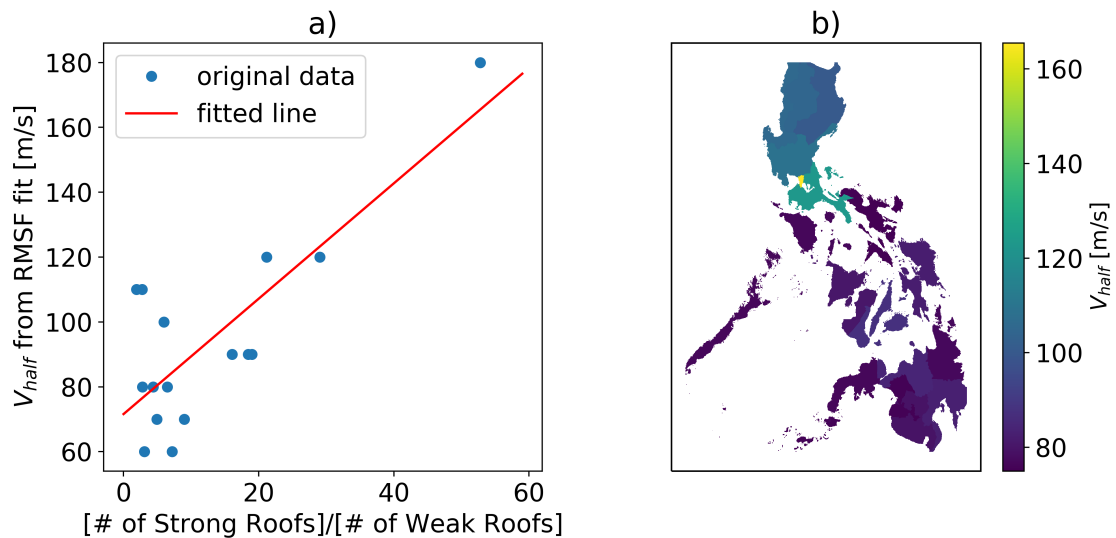
1109 FIG. 9. **Simulated versus observed asset losses with a single national vulnerability curve fit to minimize**  
 1110 **RMSE.** Observed total damages are plotted against modeled total damages with (a) linear axes and (b) log-scale  
 1111 axes (b); black lines are one-to-one lines and events that result in losses in Manila are encircled in blue. (c) Bar  
 1112 chart of number of TC events with damage ratios less than 0.1, between 0.1 and 10, and greater than 10, split into  
 1113 events that do not affect Manila (orange) versus those that do affect Manila (blue). As a reminder, event damage  
 1114 ratio is equal to simulated damages for a TC divided by normalized reported damages for the same TC.



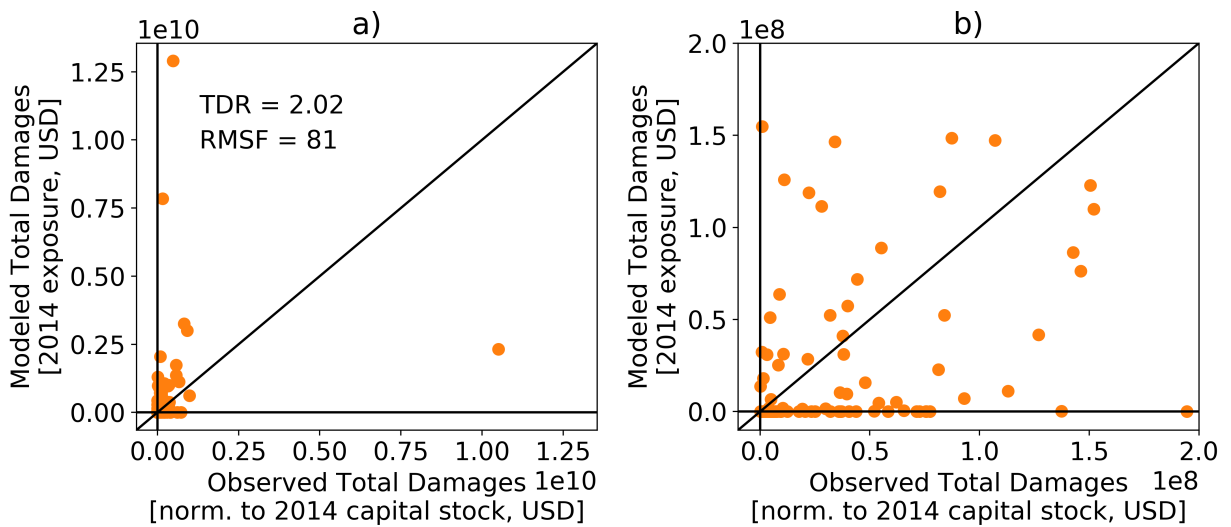
1115 **FIG. 10. Prevalence of different roof materials for regions in the Philippines.** Bar charts for each region  
 1116 showing percent of population occupying dwellings made of different roof materials, according to the Philippines  
 1117 household survey data (FIES). The key in grey shows what roof materials each x-axis number represents.



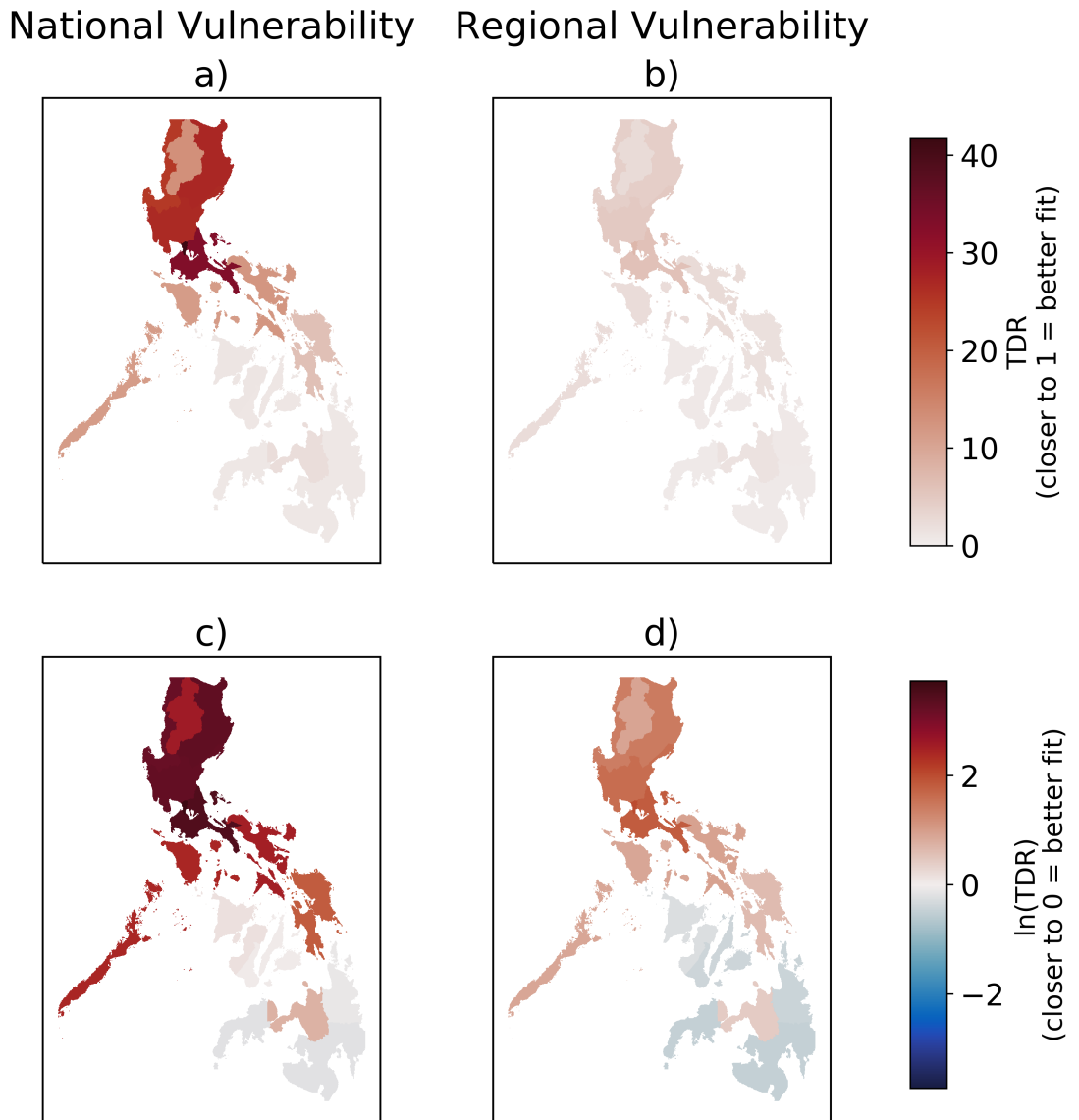
1118 FIG. 11. **Proportion of strong to weak roofs for regions in the Philippines.** Bar chart showing number of  
 1119 strong divided by number of light roofs for each region in the Philippines.



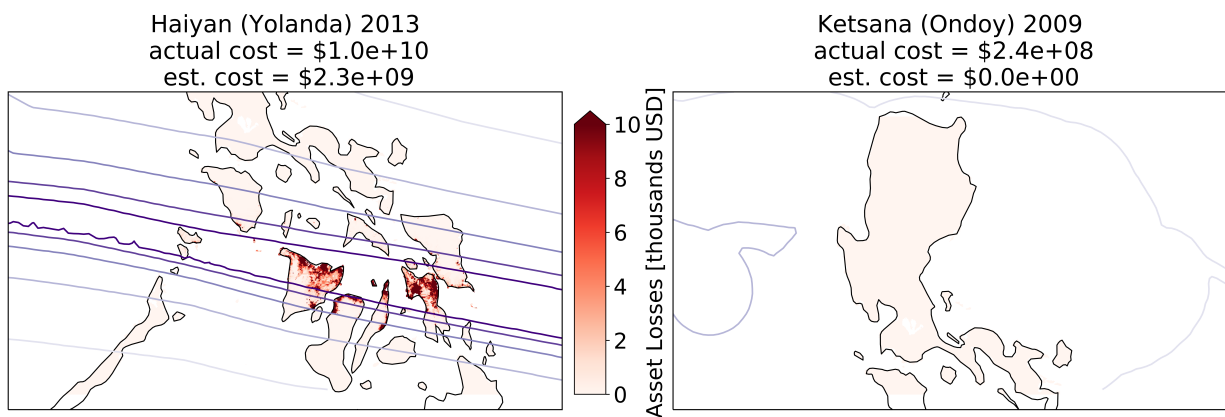
1120 FIG. 12. **Correspondence of regional  $V_{half}$  to roof strength proportion, and resulting vulnerability map**  
 1121 **from regression.** (a) Proportion of strong to weak roofs plotted against RMSF fitted regional  $V_{half}$  values (blue  
 1122 circles) and linear fit between the two quantities (red line); (b) regional  $V_{half}$  determined from proportion of  
 1123 strong to weak roofs in each province and linear fit in panel a. Note that in panel a, NCR is the top-right point in  
 1124 the plot with the highest  $V_{half}$  and strong roof proportion.



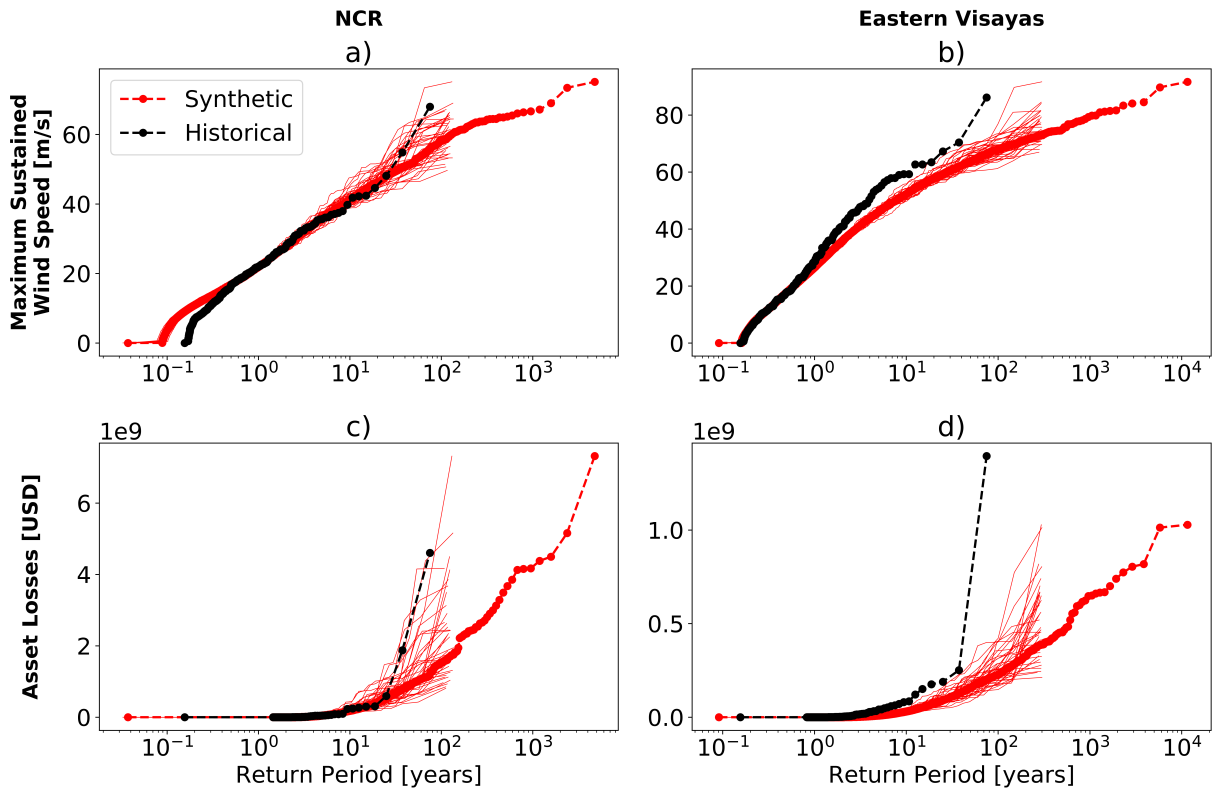
1125 **FIG. 13. Observed versus modeled damages for regionally varying vulnerability.** (a) Observed total  
 1126 damages from EM-DAT plotted against modeled total damages calculated with the regional varying vulnerability  
 1127 map; black line is the one-to-one line. (b) Same as panel a but with reduced x and y-axis limits to highlight the  
 1128 prevalence of storms with zero modeled damages.



1129      FIG. 14. **Damage simulation skill for national versus regionally varying vulnerability.** TDR across regions  
 1130      for single national vulnerability curve (left) and regionally varying vulnerability curves (right) and quantified as  
 1131      raw TDR (top) versus natural log of TDR (bottom).



1132 **FIG. 15. Wind swath and asset losses for two notable Philippines-landfalling typhoons.** Wind swath  
 1133 (contoured in purple— darker contours corresponds to faster wind speeds) and damages (shaded red)  
 1134 typhoon Haiyan (Yolanda) and (right) Ketsana (Ondoy). The plot region is constrained to the area of most direct  
 1135 impact by each storm, and at the top of each plot the actual cost from EM-DAT is listed above the simulated  
 1136 damages summed across the entire Philippines.



1137 FIG. 16. **Return periods for wind speed and asset losses for two regions in the Philippines.** Return periods  
 1138 of different (top) maximum sustained wind speeds and (bottom) asset losses, for two regions: (left) Manila/NCR  
 1139 and (right) Eastern Visayas. Simulated damages from IBTrACS tracks are shown in black, while simulated  
 1140 damages from CHAZ tracks are shown in red; the thin red lines designate return periods derived from each  
 1141 CHAZ intensity ensemble while the thick dashed red line shows return periods from all the CHAZ tracks and  
 1142 intensity ensembles together.